

WMO/TCP/WWW
NINTH INTERNATIONAL WORKSHOP
ON TROPICAL CYCLONES
(IWTC-9)

Subtopic 4.3. Extratropical Transition

Rapporteur: Ron MCTAGGART-COWAN
Environment and Climate Change Canada
ron.mctaggart-cowan@canada.ca
+1 514-421-7268

Rapporteur: Clark EVANS
University of Wisconsin-Milwaukee
evans36@uwm.edu
+1 414-229-4469

Working Group

Sim Aberson, Heather Archambault, Lance Bosart, Suzana Camargo, Jim Doyle, Peter Finocchio, John Gyakum, Naoko Kitabatake, Thomas Loridan, Florian Pantillon, Julian Quinting, Carolyn Reynolds, Elizabeth Ritchie, Ryan Torn, Colin Zarzycki

Abstract

This report builds on two recent review papers in *Monthly Weather Review* (Evans et al. 2017, Keller et al. 2019) to document recent advances in the field's understanding of extratropical transition. Significant advances have been made in our understanding of structural evolution during the transformation stage of extratropical transition, fostered in large part by *in situ* observations collected during earlier field campaigns. These *in situ* observations have also been leveraged to help document forecast sensitivities associated with, and the practical predictability of, extratropical transition. The last four years have also seen many of the first studies in which recent and projected changes in extratropical transition climatologies have been examined. The most substantial gains in insight since the last IWTC have arguably come, however, in the field's understanding of midlatitude flow interaction, downstream development, and the associated high-impact weather that can result from extratropical transition events. These findings and recommendations for future research, particularly to benefit operational forecasting centers, are documented herein.

4.3.1 Introduction

The process by which tropical cyclones (TCs) transition into baroclinic cyclones as they recurve into the midlatitudes is known as extratropical transition (ET). Most affected by ET are the North Atlantic and western North and South Pacific basins during the "shoulder" seasons, when the equatorward displacement of the baroclinic westerlies

favors interactions between TCs and Rossby waves propagating along the midlatitude jets or “waveguides”. Storms undergoing ET pose a particular forecasting challenge because of the rapid structural and track changes that occur during this stage of the storm lifecycle. This predictability problem is compounded by the fact that the poleward movement of transitioning storms means that they affect regions in which the infrastructure and the population is not well prepared for the severe TC-like impacts that these storms can produce.

A pair of very recent review articles serves to document the current state-of-the-art in ET research and forecasting (Evans et al. 2017; Keller et al. 2019). Although the research described in this report is necessarily based on work that was in progress during the preparation of the review papers, the focus here on only the most recent investigations (2014 onwards) distinguishes this report from the reviews. Additionally, the design of this report departs from the structure of the review papers in a way that is intended to make the current work a useful reference for readers looking for an overview of current ET research and for proposals for near-term investigations that will advance the community’s understanding of ET going forward.

The distinguishing characteristic of ET is the structural change of the remnant TC from a symmetric, warm-core vortex to an asymmetric, cold-core circulation with well-defined frontal features. Associated with this structural change is the transition of the primary energy source for the system from surface enthalpy fluxes to the large-scale baroclinic conversions germane to midlatitude cyclones. This dramatic evolution in the nature of the storm brings with it serious predictability challenges, especially because of the sensitivity of ET to the structure of the midlatitude flow into which the TC remnant recurves. Depending on the state of the midlatitude jet, the impact of ET on this waveguide varies from a slight intensification of the jet core to the development of a high-amplitude Rossby wave train that can lead to multiple high-impact weather events downstream. The prediction of specific basin-scale outcomes from ET in both weather and climate models is at once challenging and essential, not the least because of the economic and societal costs that these events can incur.

All of these aspects of the ET problem will be addressed in this report. In section 4.3.2, we review recent work regarding the structural changes that occur during ET. This perspective is expanded to the basin scale in section 4.3.3, which considers interactions between the transitioning TC and the midlatitude waveguide, downstream development and downstream high impact weather. A discussion of the associated predictability limits and current forecast skill for transitioning storms and their downstream impacts follows in section 4.3.4. This builds towards the descriptions in section 4.3.5 of recent advances in understanding ET in a climatological context. In section 4.3.6, the report concludes with a summary of ongoing investigations, a review of gaps in our knowledge, and recommendations for research topics that may be particularly valuable to the ET research community, operational forecasters, decision-makers and stakeholders in affected areas.

4.3.2 Structural Evolution

As discussed in the recent ET review (Evans et al. 2017), a TC that travels poleward into a baroclinic environment with its attendant temperature and moisture gradients typically undergoes a structural change from a deep warm-core cyclone into

either a shallow warm-core or a deep cold-core cyclone, with an asymmetric, frontal structure (e.g., Hart et al. 2006; Klein et al. 2000). Specifically, as TC moves poleward and the transformation stage of ET begins, its outer circulation encounters a midlatitude baroclinic zone, and the deep, moist convection of the inner-core becomes increasingly asymmetric. Subsequently, as the TC becomes collocated with and embedded into the baroclinic zone, the TC acquires substantial vertical tilt, develops features such as the conveyor belts characteristic of extratropical cyclones, and thunderstorm activity becomes isolated some distance poleward of the center (Klein et al. 2000; Ritchie and Elsberry 2001).

Likewise, during the transformation stage, the cyclone's near-surface wind field becomes asymmetric and grows (Evans and Hart 2008), resulting in an increase of the cyclone's integrated kinetic energy (Kozar and Misra 2014). Concurrently, precipitation fields become asymmetric and expand radially with increased areal coverage (Matyas 2013). The heaviest precipitation becomes located downshear of the circulation center and may occur either left- or right-of-track (Atallah et al. 2007; Milrad et al. 2009), with left-of-track rainfall favored in environments favoring cyclone reintensification (i.e., a negatively tilted trough upshear of the TC). The locations of heaviest precipitation during ET are further modulated by orography, with maximum amounts located in areas of upslope flow (Liu and Smith 2016; Keighton et al. 2016) or areas of orographically driven ageostrophic frontogenesis (Milrad et al. 2013).

In the following, advances in understanding of structural evolution during ET since the last IWTC are documented. Perhaps most significant of these is the first observational confirmation of the earlier conceptual models of structural evolution, as discussed in the next subsection.

a) Observations of Structural Evolution

Several recent field campaigns have provided novel observations of transitioning TCs (Wu et al. 2005; Waliser et al. 2012; Rogers et al. 2013; Schäfler et al. 2018). Since 2014, observations from these campaigns – particularly the THORPEX Pacific Asian Regional Campaign (T-PARC; Waliser et al. 2012) – have helped confirm the validity of conceptual models of the transformation stage of ET previously developed by Klein et al. (2000) and Ritchie and Elsberry (2001).

During step 1 of the transformation stage, the TC translates poleward, its outer circulation encounters a midlatitude baroclinic zone, and the deep, moist convection of the inner core becomes more asymmetric, with an associated wavenumber-one asymmetry in the vertical motion and radar reflectivity fields with maximum ascent and reflectivity downshear-left, and maximum descent and minimum reflectivity in the upshear semicircle. Based on an analysis of Doppler radar, dropsonde, aircraft flight level, and satellite atmospheric motion vector data from western north Pacific Typhoon Sinlaku in 2008, these asymmetries have been attributed to the environmental deep-layer vertical wind shear (Foerster et al. 2014). Consistent with balanced dynamics, this deep-layer vertical wind shear led to predominantly upward mass flux downshear and downward mass flux upshear. Convective cells formed downshear-right (Fig. 4.3.2.1d), rotated cyclonically downstream, reached maximum intensity downshear-left (Fig. 4.3.2.1b), and decayed upstream (Fig. 4.3.2.1a and c). This pattern is consistent with previous theoretical, observational, and model studies of TCs in vertical shear (e.g.,

Marks et al. 1992; Frank and Ritchie 2001; Black et al. 2002; Corbosiero and Molinari 2002; Reasor et al. 2009; DeHart et al. 2014).

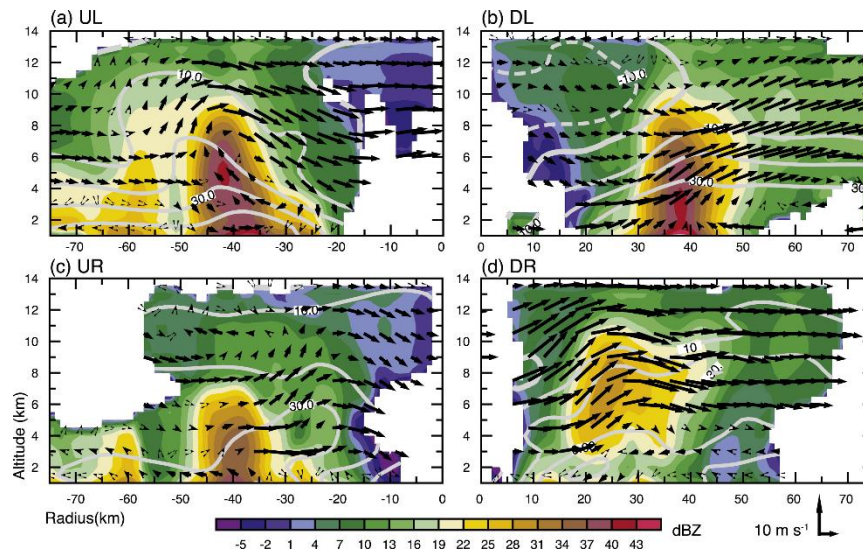


Fig. 4.3.2.1. Vertical cross-sections through Typhoon Sinlaku of radar reflectivity in dBZ (shaded), tangential wind in m s^{-1} (gray contours), and in-plane wind vectors composed of radial and vertical velocity for each shear-relative quadrant. Cross-sections are taken from the corner of the domain to the center, 45° from the x - and y - axes in each quadrant: (a) upshear left, (b) downshear left, (c) upshear right, and (d) downshear right. Figure reproduced from Foerster et al. (2014).

During step 2 of the transformation stage, the TC becomes superposed on the midlatitude baroclinic zone. Observational studies indicate that processes associated with this superposition, rather than a response to vertical wind shear, are the cause of asymmetries in the cyclone structure during this stage (Quinting et al. 2014, Katsumata et al. 2016). Warm frontal development east of the transitioning cyclone leads to forced ascent (Fig. 4.3.2.2), in turn triggering deep, moist convection and the formation of a broad stratiform precipitation region that causes heavy precipitation to the northeast of the transitioning TC. Though latent heat release due to condensation may enhance the remnant circulation of the TC aloft (Quinting et al. 2014), cooling due to evaporation and melting in the dry, cool air north of the warm front may enhance lower-level frontogenesis, potentially contributing to increased precipitation (Katsumata et al. 2016). On the western flank of the cyclone, cold frontal development is weak, and deep, moist convection is suppressed due to warm and dry air aloft and cold air near the surface.

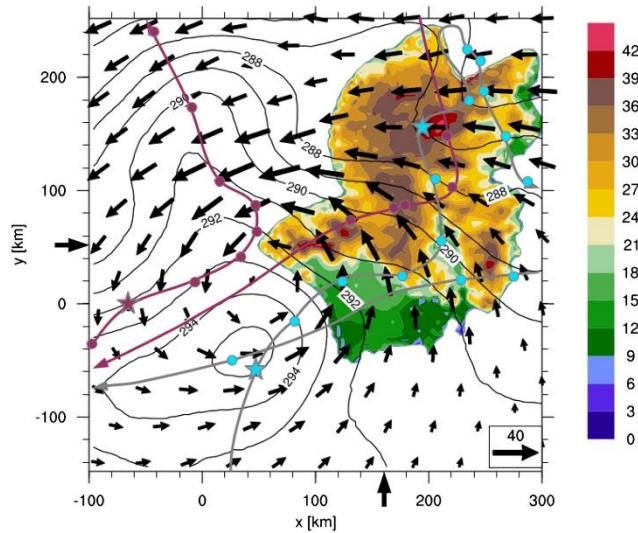


Fig. 4.3.2.2. Overview of the analyzed domain and the spatial distribution of observational data. Maximum reflectivities between 0 and 15 km (dBZ; shaded) and temperature (K; contours) at 1.5 km. Wind vectors give horizontal wind at 1.5 km (m s^{-1}). Gray line denotes flight track of the NRL-P3 and red line denotes flight track of the USAF-WC130. Filled circles give positions of dropsondes included in SAMURAI analysis. Stars indicate positions of dropsondes in Fig. 7 in Quinting et al. (2014). Black arrows at coordinate axis show positions of cross-sections in Fig. 6 of Quinting et al. (2014).

b) Wind Field Evolution

The hazard risk from TCs is multi-faceted, with strong winds, large waves, and storm surge all posing significant threats. The nature of these threats changes during ET, however, as the wind field structure changes (Bruneau et al. 2017; Evans et al. 2017). New research since the last IWTC has sought to quantify the variability in ET-related near-surface wind field structures and develop improved parametric and statistical models for wind field structure during ET (Loridan et al. 2014, 2015, 2017).

A long-accepted framework to conceptualize TC surface level winds has been that they result from the superposition of a symmetric vortex (e.g., Holland 1980; Willoughby et al. 2006) with the TC's forward motion. This framework depicts TCs as translating systems with strongest winds found to the right of motion in the Northern Hemisphere and to the left of motion in the Southern Hemisphere. In terms of risk assessment, this puts one side of the TC track at a much higher risk than the other. Using aircraft observations from 128 flights into tropical cyclones, Uhlhorn et al. (2014) found that while this paradigm is largely accurate at flight level, it fails near the surface where it is needed the most for risk assessment. They conclude that surface wind asymmetry is related to deep-layer shear rather than storm motion, with the strongest near-surface winds generally located downshear-left of the center. This asymmetry tends to shift downwind during ET as baroclinicity and shear increase. The limitations of the symmetric superposition framework during ET have also been highlighted by Kitabatake and Fujibe (2009) and Loridan et al. (2014). Both investigations showed that it is common for ET cases to have similar wind risk on both sides of the transitioning TC (e.g., Fig. 4.3.2.3), with approximately 67% of TCs that complete ET near Japan having

winds to the left-of-track that are within 20% of those to the right-of-track (Loridan et al. 2014).

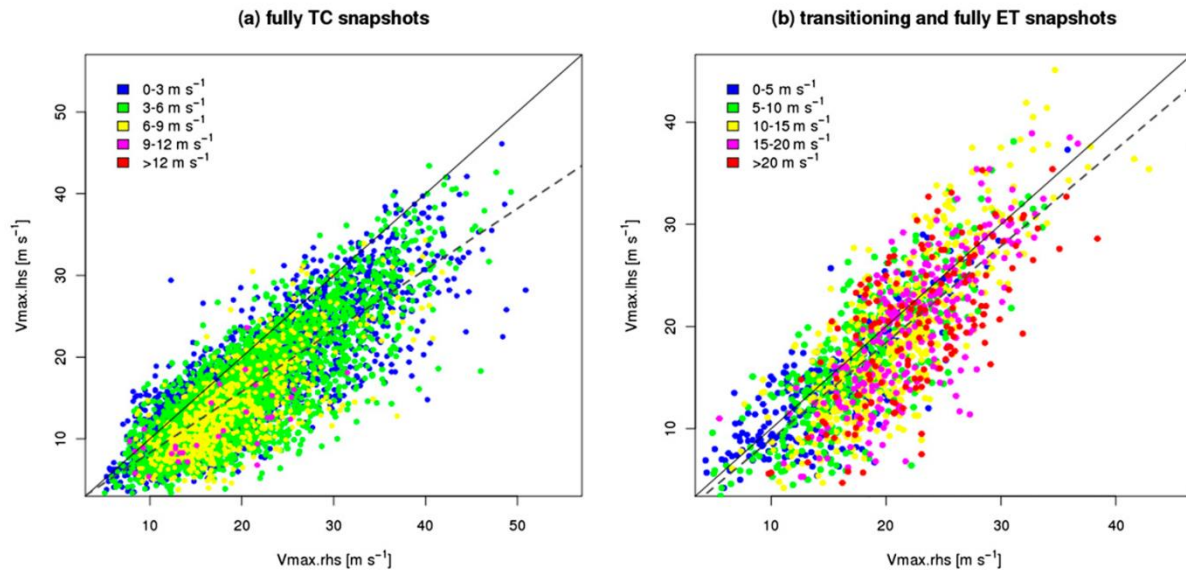


Fig. 4.3.2.3. Maximum 10-m wind speed to the left of motion ($V_{\max.lhs}$; y-axis) as a function of the maximum to the right of motion ($V_{\max.rhs}$; x-axis) in the western North Pacific Ocean. Color bins indicate the storm translational speed. The 1:1 (solid) and linear regression (dashed) lines are shown. See Loridan et al. (2014) for more details.

Although traditional parametric modeling solutions built for pure tropical cyclones are not adequate for ET cases, research in developing alternative methods has been limited to date. Loridan et al. (2015) propose an extension to the Willoughby (2006) model that specifically implements a left-of-track wind maximum component for the ET phase in the western North Pacific. This model is able to replicate an ET-specific surface wind structure (Fig. 4.3.2.4), yet its implementation as part of a risk assessment system is complex because it requires input from a separate model to determine if the TC is undergoing ET or not. Knaff et al. (2017) develop a hybrid statistical-dynamical model that provides skillful estimates for wind radii around storm centers for a 2-year sample of storms across the major TC basins. However, they also conclude that ET poses a unique challenge for wind field prediction.

More recently, a machine-learning model that has been trained on a large database of realistic high-resolution TC wind structures has been developed and applied to extract automatically the most relevant wind field asymmetry patterns (Loridan et al. 2017). The spatial wind distribution can then be modeled from these patterns given knowledge of the TC track, intensity, and wind field extent. Since the training database includes both pure TCs as well as ET cases, the machine-learning model learns to model both types of structure in a unified framework. However, assembling a larger, global catalog of TCs would enable the machine-learning model to learn from and better represent a broader range of TC features, including the complex wind field structures that develop during ET.

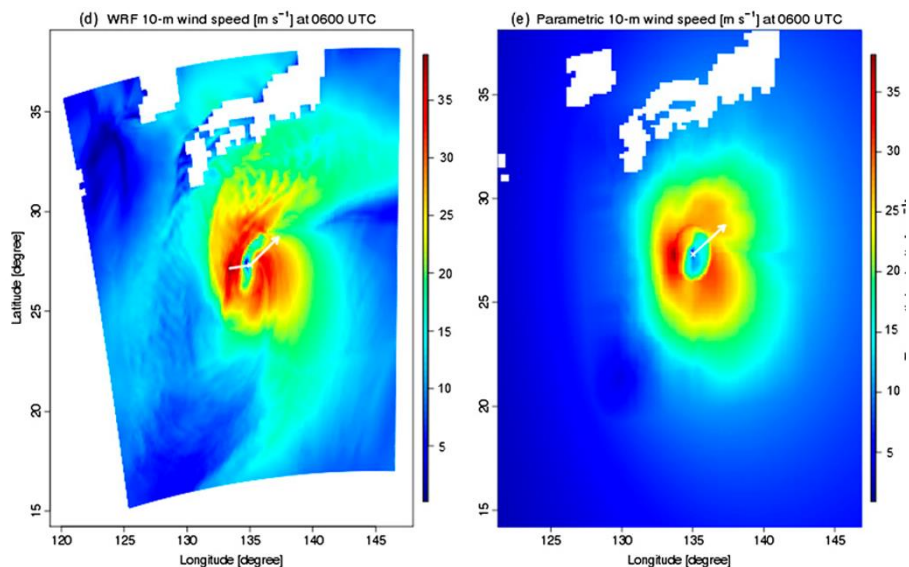


Fig. 4.3.2.4. WRF-ARW-simulated 10-m wind speed (in m s^{-1}) for Typhoon Rammasun at 0600 UTC 12 May 2008 (left) and the corresponding 10-m wind speeds from the Loridan et al. (2015) ET model (right).

c) Precipitation Evolution

Rainfall with ET events may be *directly* – e.g., resulting from the direct interaction of the TC with the midlatitude baroclinic zone – or *indirectly* – e.g., such as in the case of a predecessor rain event (PRE; e.g., Galarneau et al. 2010) – related to the transitioning TC. Since the last IWTC, advances in understanding for both rainfall event types have been made. The importance of these findings lies in their societal impacts to regions that do not necessarily receive frequent direct TC impacts. For example, a recent statistical analysis of heavy rain events in a reservoir in New York state finds that TCs are a large fraction of heavy rainfall events in the area, with ET events making up 70% of the TC total (Towey et al. 2018). In the following, advances in understanding of both direct and indirect TC-related rainfall before and during ET are discussed.

Studies during the past four years have shown that the *amount* of rainfall directly associated with ET events is related to environmental factors including the amount of environmental moisture (Matyas 2017), the strength of the midlatitude baroclinic zone and its proximity to the TC during ET, the strength of moisture and temperature advection during ET (and associated frontogenesis and forcing for ascent on sloped isentropic surfaces), and the alignment of the motion and vertical wind shear vectors (Deng and Ritchie 2018a).

The *pattern* of rainfall directly associated with ET events is also related to interaction with topography (e.g., Milrad et al. 2013, Liu and Smith 2016, Keighton et al. 2016), the strength of the midlatitude baroclinic zone and its proximity to the transitioning TC, moisture and temperature advection strength, the ascent of moist air along sloping isentropes poleward and downstream of the TC, and the alignment of the motion and vertical wind shear vectors (Deng and Ritchie 2018a). Both rainfall coverage

and asymmetry (left-of-track vs. right-of-track) are affected by these factors. The latter can be quantified by a rainfall metric B_{rain} (Deng and Ritchie 2018b), which is closely related to the lower-tropospheric thermal asymmetry parameter B of the cyclone phase space of Hart (2003).

A case study of a heavy rainfall event directly associated with an ET event was performed for Typhoon Etau (2015) by Kitabatake et al. (2017). A meridionally oriented rainband (black bar in Fig. 4.3.2.5) became organized east of Etau (A in Fig. 4.3.2.5) after it completed ET. This rainband was responsible for heavy rainfall over eastern Japan, with total precipitation exceeding 500 mm. After Etau completed ET, two middle tropospheric cyclonic potential vorticity (PV) anomalies (B and C in Fig. 4.3.2.5) that had origins in the upper troposphere in the midlatitudes moved southeastward, were cyclonically advected around Etau, and eventually reached the area of heaviest rainfall. These disturbances were associated with mid-tropospheric dry air and forcing for ascent, resulting in the realization of potential instability and heavy rain.

Indirect rainfall, or that falling well ahead of the TC during ET, has been recently studied over the Korean Peninsula (Baek et al. 2015). Over a twenty-two-year sample, antecedent indirect precipitation ahead of the transitioning TC was found to be related to the development of middle tropospheric frontogenesis as the TC interacted with the midlatitude environment. Although Baek et al. (2015) conclude that antecedent indirect precipitation is different from the PREs defined by Galarneau et al. (2010) because frontogenesis is focused at mid-levels rather than the surface, the original definition of a PRE does not depend on the mechanism forcing ascent. This is reinforced by Galarneau (2015), who investigated the impact of an oceanic PRE on the track of TC Isaac (2012). Galarneau (2015) shows that mid- and upper-level frontogenesis provided the forcing for moist ascent in this case, with structures like those found over Korea by Baek et al. (2015). Given that there is no reason to expect that fundamentally different processes occur in different regions to trigger remote precipitation events, use of consistent terminology would avoid the divergence of studies on this form of indirect TC-related rainfall and ease future literature reviews. Because the PRE terminology appeared first in the literature, it should be preferred in future works investigating this topic.

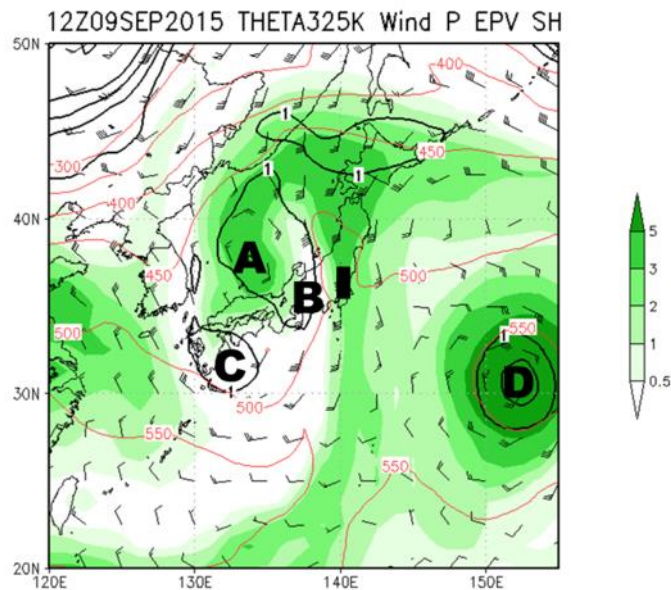


Fig. 4.3.2.5. 325-K isentropic surface analysis at 1200 UTC 9 September 2015, including isentropic potential vorticity (black line, PVU), pressure (red line, hPa), specific humidity (shaded, g kg^{-1}), and wind (barb; half-barb: 5 kt, barb: 10 kt, pennant: 50 kt). The black bar near the center of the figure shows the axis of the heavy rainfall. After Kitabatake et al. (2017).

4.3.3 Trough Interaction and Downstream Development

Prior to 2014, idealized and real case studies revealed that the phasing and interaction of a transitioning TC with an upstream trough is crucial for the development of the transitioning TC and its downstream impact (Ritchie and Elsberry 2007; Riemer and Jones 2010; Scheck et al. 2011; Grams et al. 2013b). Recent climatological studies on western North Pacific transitioning TCs (Archambault et al. 2015; Torn and Hakim 2015; Quinting and Jones 2016) corroborate these findings, emphasizing the importance of divergent outflow to downstream development.

Specifically, upper-tropospheric potential vorticity advection by the divergent component of the wind typically strengthens the local extratropical potential vorticity gradient (or waveguide), intensifying the jet streak between the upstream trough and downstream ridge, and amplifies the downstream ridge by deforming potential vorticity contours poleward. This process may impede the upstream trough's eastward propagation, contributing to the favorable phasing of the TC with the upstream trough (Griffin and Bosart 2014; Pantillon et al. 2015; Archambault et al. 2015; Quinting and Jones 2016). This non-linear interaction results in a more poleward track of the TCs (Quinting and Jones 2016) and a stronger amplification of the downstream flow (Chen et al. 2017).

a) Downstream Development

During ET, quasi-geostrophic forcing for ascent provided by the upstream trough leads to the ascent of warm and moist tropical air masses that have been transported poleward towards the midlatitude baroclinic zone by the cyclonic TC circulation (Quinting and Jones 2016; Grams and Archambault 2016; Riboldi et al. 2018). Of note, this transport is significantly stronger than that associated with extratropical cyclones, particularly for western North Pacific TCs (Torn and Hakim 2015). Ascent may occur several days (500-2000 km) ahead of, or in direct association with, the transitioning TC. In the former case, it is known as a predecessor rain event (section 4.3.2c). Ascent directly associated with the transitioning TC may be upright or slantwise, with the former dominating as ET begins and the latter becoming increasingly common at later times (Grams et al. 2013a; Grams and Archambault 2016). This ascent is maximized poleward of the TC and ahead of the upstream trough in the equatorward entrance region of an anticyclonically curved jet streak and is collocated with midlevel frontogenesis (Archambault et al. 2015; Grams and Archambault 2016).

The ascent resulting from the non-linear interaction between the TC, upstream trough, and the midlatitude baroclinic zone manifests itself in an upper-tropospheric divergent flow. Though it has not yet been rigorously tested, it is assumed that the divergent outflow during ET is mostly driven by latent heat release. Initial estimates using the quasigeostrophic omega equation corroborate this assumption (Quinting and Jones 2016), and poleward moisture transport (which can be thought of as a proxy for latent heat release upon ascent) is crucial to downstream ridge amplification and Rossby wave packet initiation (Riboldi et al. 2018).

The ridge amplification that often occurs downstream of transitioning TCs has been the focus of numerous recent case and composite studies (Griffin and Bosart 2014; Keller et al. 2014; Torn et al. 2015; Grams and Archambault 2016; Keller 2017), idealized simulation evaluations (Riemer and Jones 2014), and climatological studies (Archambault et al. 2015; Torn and Hakim 2015; Quinting and Jones 2016; Riboldi et al. 2018). Based on studies conducted prior to 2014 and the studies cited above, a consistent picture has emerged. In the following, this picture is described using two complementary frameworks: eddy kinetic energy and potential vorticity.

In the eddy kinetic energy framework, eddy available potential energy is converted to eddy kinetic energy through the ascent of the poleward-transported warm air mass (Keller et al. 2014; Quinting and Jones 2016; Keller 2017). The newly generated eddy kinetic energy is redistributed by ageostrophic geopotential fluxes to the downstream ridge's flanks, with the local accumulation of eddy kinetic energy on the downstream ridge's western flank driven by converging ageostrophic winds (due to the upstream trough) and divergent flow resulting from diabatically driven ascent along the midlatitude baroclinic zone (e.g., Chen 2015; Quinting and Jones 2016; Keller 2017). Eddy kinetic energy is subsequently dispersed by ageostrophic geopotential fluxes to downstream regions, where it contributes to the formation of further eddy kinetic energy maxima on the flanks of downstream troughs and ridges. The ageostrophic geopotential flux convergence magnitude on the western flank of the downstream ridge is directly proportional to the magnitude of the evolving Rossby wave packet (Quinting and Jones 2016; Keller 2017).

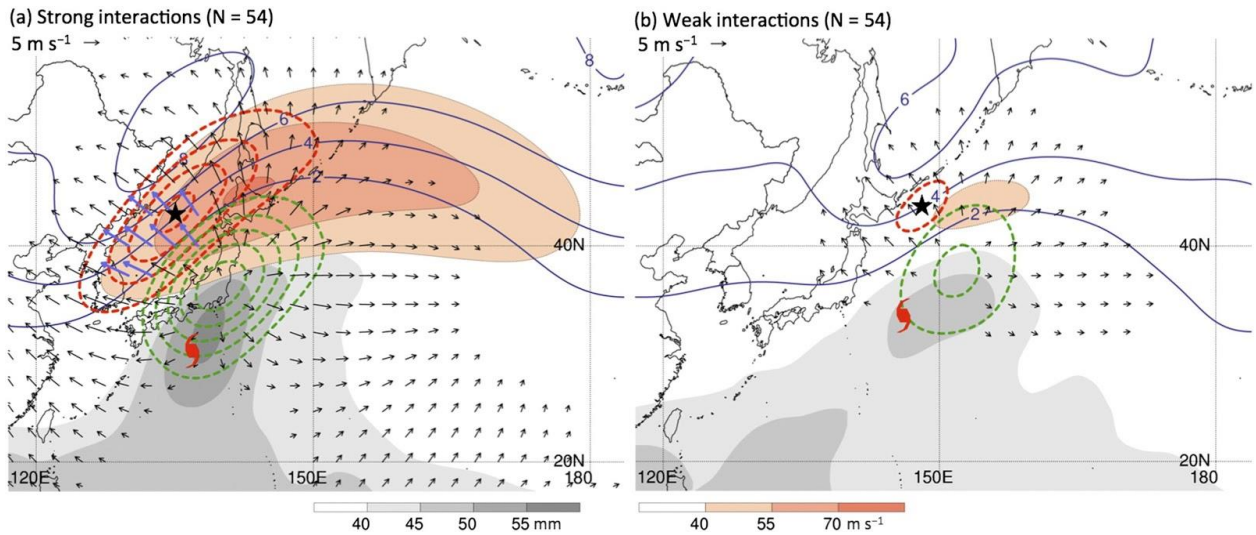


Fig. 4.3.3.1. Composite analyses showing (a) strong and (b) weak TC–extratropical flow interactions. Analyses show 500-hPa ascent (dashed green, every 2×10^{-3} hPa s^{-1} , negative values only), precipitable water (shaded according to grayscale, mm), 200-hPa PV (blue, every 1 PVU), irrotational wind (vectors, > 2 m s^{-1} ; purple vectors, > 8 m s^{-1}), negative PV advection by the irrotational wind (dashed red, every 2 PVU day^{-1} starting at -2 PVU day^{-1}), and total wind speed (shaded according to color bar, m s^{-1}). The star denotes the composite point of maximum interaction (strongest instantaneous negative PV advection by the irrotational wind). The TC symbol denotes the composite TC position. Reproduced from Archambault et al. (2015).

In the potential vorticity (PV) framework, divergent outflow impinges on the PV gradient coincident with the midlatitude jet stream, displaces it poleward, and thus contributes to the downstream ridge amplification (Figs. 4.3.3.1 and 4.3.3.2; Griffin and Bosart 2014; Archambault et al. 2015; Torn et al. 2015; Quinting and Jones 2016; Grams and Archambault 2016; Riboldi et al. 2018). The upstream jet streak forms due to upper-tropospheric frontogenesis as the divergent outflow strengthens the midlatitude PV gradient (Archambault et al. 2015). In the presence of a PRE, the related divergent outflow may contribute to an initial amplification of the downstream ridge, which may be thought of as environmental preconditioning (Fig. 4.3.3.2a; Grams and Archambault 2016; Bosart et al. 2017). Overall, a broad consensus in current ET research is that the upper-tropospheric divergent outflow has the largest individual contribution to the downstream ridge building. However, as the TC approaches the midlatitude PV gradient during ET, the contribution of the transitioning cyclone’s circulation to downstream ridge amplification increases (Riemer and Jones 2014; Quinting and Jones 2016), although recent research suggests that downstream ridge amplification is not directly related to the transitioning cyclone’s intensity (Archambault et al. 2015; Quinting and Jones 2016; Chen et al. 2017; Riboldi et al. 2018).

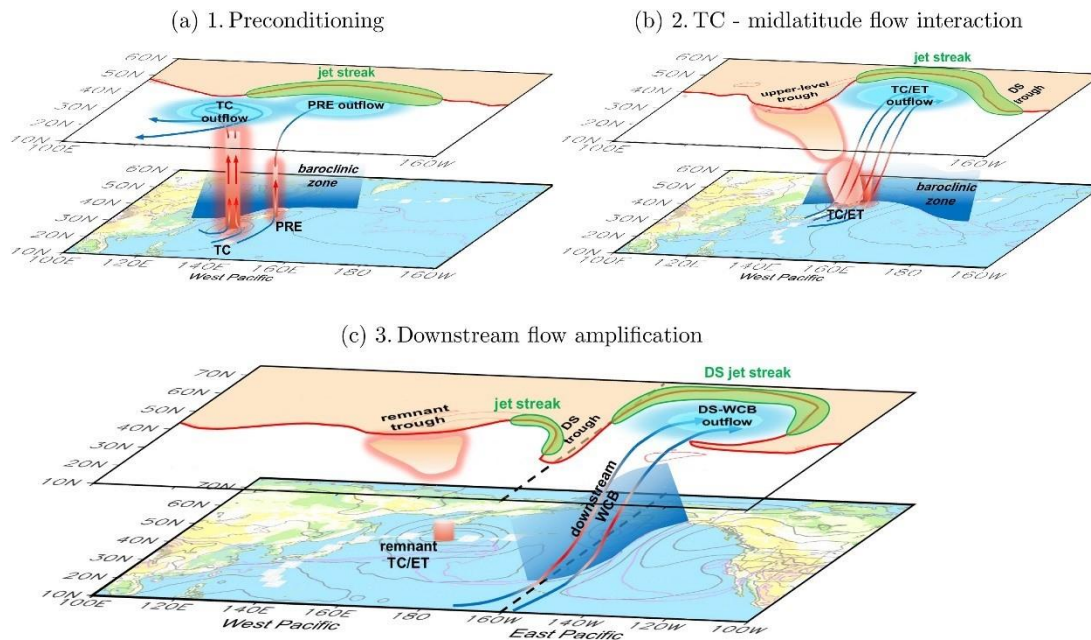


Fig. 4.3.3.2. Schematic of the three stages of ET. Red objects indicate positive PV associated with the transitioning TC and PRE. Light blue regions at upper levels indicate low-PV air in the outflow of the weather systems. The jet streaks are indicated in green, the upper-level waveguide (3 PVU) with a red contour, and orange shading is to the north. Dark blue tilted surfaces indicate low- and mid-level baroclinic zones. Trajectories of rapidly ascending air parcels are indicated by blue-red-blue lines, reflecting the diabatic PV modification. (a) Preconditioning stage of ET with contours at lower surfaces showing mean sea level pressure (black) and equivalent potential temperature (violet), as well as contours at the upper surface showing 3 PVU at 200 hPa at $t+12$ h. (b) The TC-extratropical flow interaction stage of ET showing the same fields as in (a), but at $t+60$ h and 3 PVU at 335 K. (c) The downstream flow amplification stage of ET showing the same fields as in (b), but at $t+108$ h. From Grams and Archambault (2016).

Further downstream, Rossby wave dispersion and the equatorward advection of anomalous cyclonic PV (induced by the anticyclonic wind field associated with the downstream ridge and the outflow anticyclone associated with the TC) result in the development of a trough downstream of the transitioning cyclone and downstream ridge (Riemer and Jones 2014; Grams and Blumer 2015; Grams and Archambault 2016). This downstream trough triggers downstream lower-tropospheric cyclogenesis, with the resulting cyclone itself associated with the poleward transport of warm and moist air (i.e., manifest as a warm conveyor belt). This contributes to ridge amplification further downstream (Fig. 4.3.3.2c; Grams and Archambault 2016), with impacts to hemispheric weather on the synoptic to sub-seasonal scales (~ 7 -14 days; Archambault et al. 2015).

In a climatological sense, downstream development characteristics vary slightly between basins. For example, Rossby wave packets associated with downstream development are stronger (i.e., of higher amplitude) and occur more frequently than climatology downstream of transitioning TCs in the western North Pacific and southwest Indian oceans (e.g., Archambault et al. 2013, 2015; Torn and Hakim 2015; Quinting and

Jones 2016), but not in the North Atlantic Ocean (Quinting and Jones 2016). This is hypothesized to result from a comparatively short and weak climatological waveguide over the North Atlantic Ocean which may favor downstream anticyclonic Rossby wave breaking that can disrupt downstream development (Archambault et al. 2015). This is consistent with earlier case studies that were unable to systematically attribute RWP amplification to North Atlantic TCs (e.g., Agusti-Panareda et al. 2004; Pantillon et al. 2015). In the western North Pacific, it is also possible for transitioning TCs to interact with, and perturb, a zonally aligned midlatitude flow. Such a configuration is also associated with a higher-than-normal probability of downstream development as compared to climatology (Riboldi et al. 2018), although the flow perturbations are stronger and longer-lasting in the presence of a preexisting midlatitude trough (Fig. 4.3.3.3; Archambault et al. 2015; Torn and Hakim 2015; Quinting and Jones 2016).

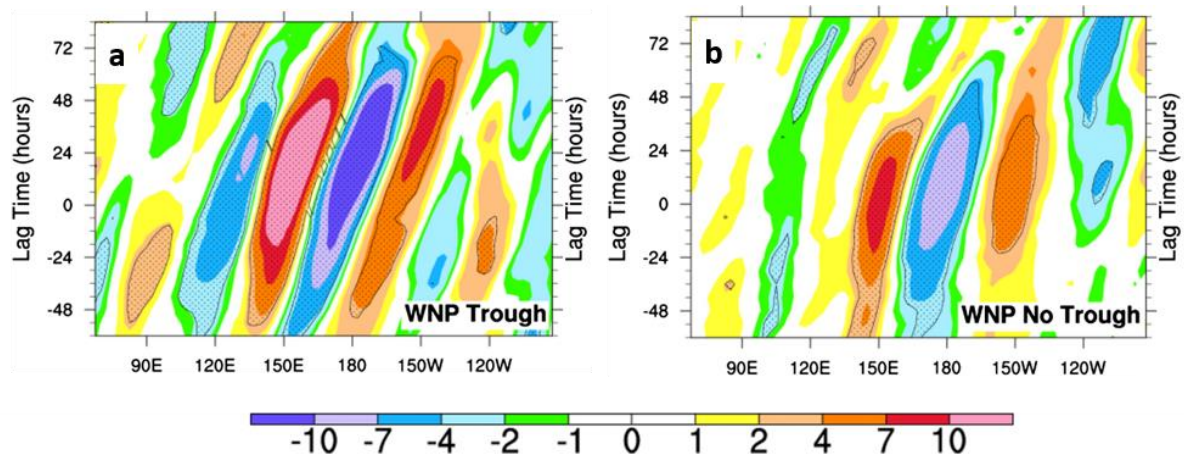


Fig. 4.3.3.3. Meridional wind anomalies averaged between 35° and 55°N for western North Pacific (WNP) ET cases (a) with and (b) without preceding upper-level trough as a function of longitude and time (shading, m s^{-1}), where stippled regions denote where the value is statistically significant at the 95% level. From Torn and Hakim (2015).

b) High-Impact Weather

To date, most investigations of high-impact weather resulting from downstream development associated with ET have been case studies of individual events, with most focusing on transitioning western North Pacific and North Atlantic TCs. In the western North Pacific, a systematic relationship between ET events and downstream high-impact weather has not yet been established; however, in the Atlantic, the magnitude of – and the area affected by – heavy precipitation in downstream regions is significantly enhanced 2-3 days after the interaction of North Atlantic TCs with the midlatitude flow (Fig. 4.3.3.4; Pohorsky 2018). However, there is some indication that downstream impact of ET in the North Atlantic may shift the location of high-impact weather events rather than causing them to occur when they otherwise would not have occurred (Pantillon et al. 2015).

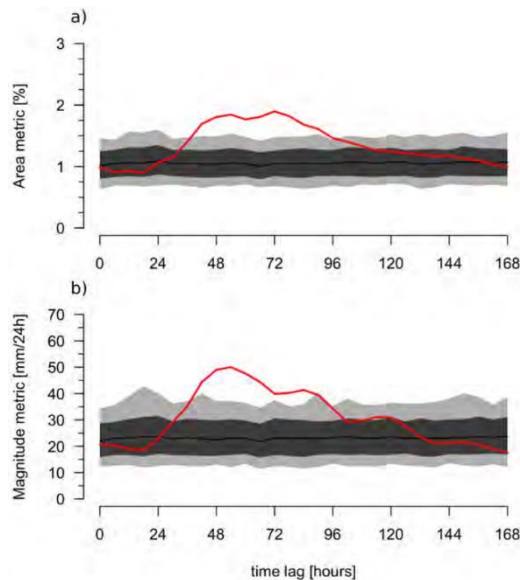


Fig. 4.3.3.4. Time series of precipitation extremes in a box 60° to 83° east of the maximum interaction point between a TC and the midlatitude flow. (a) Horizontal line represents the time lag after TC-jet interaction onsets. The vertical axis represents the fraction (%) of the box covered by precipitation extremes at a given time after the interaction. (b) Vertical axis represents the summed exceedances of the climatological 99th percentile at each grid point in the box. The red line is the average of 147 recurring north Atlantic TCs. Light and dark gray shadings respectively represent the 1st-99th and the 10th-90th intervals of precipitation extremes obtained from bootstrapping. From Pohorsky (2018).

Selected case study analyses of the downstream impact following the ET of western North Pacific and North Atlantic TCs include:

- Super Typhoon Nuri (2014)

The extratropical transition of Super Typhoon Nuri (2014) led to the formation of an omega block over western North America and several cold air outbreaks on its eastern flank (Bosart et al. 2015b).

- Tropical Storm Meari (2011)

The interaction of Meari (2011) with the midlatitude flow resulted in the amplification of a Rossby wave packet that dispersed across North America. Its dispersion contributed to the development of a trough-ridge couplet over western and central North America and the formation of two severe mesoscale convective systems over the Upper Midwest of the United States (Cordeira et al. 2017).

- Typhoon Choi-Won (2009)

Using a TC removal technique, Keller and Grams (2014) demonstrated that the ET of Choi-Won (2009) altered the severity and location of a heat wave, heavy precipitation, and a cold surge over North America.

- Typhoon Lionrock (2016)

Late in its lifecycle, Lionrock (2016) interacted with an unusually strong early-season baroclinic trough of Asian origin and associated extratropical cyclone, underwent ET, triggered a strong PRE, and generated widespread flooding across parts of Japan, Korea, China, and Russia (Bosart et al. 2018).

- Hurricane Katia (2011)

Using a TC removal technique, Grams and Blumer (2015) demonstrated that a European high-impact weather event was caused by the downstream impact of a transitioning North Atlantic TC. The interaction of Katia (2011) with the midlatitude flow caused strong upper-tropospheric ridge-building and the development of a PV streamer downstream. Deep convection and heavy rain developed in the warm and moist environment ahead of this PV streamer.

- Hurricanes Leslie, Rafael, and Sandy (2012)

Each of Leslie, Rafael, and Sandy locally impeded the forward progression of an upstream trough, then reintensified as an extratropical cyclone as the trough wrapped up. Downstream propagation characteristics of each TC's impact to the midlatitude flow vary between cases, with the common thread that all led to downstream high impact weather events that were sampled as part of SOP1 of the HyMeX field campaign (section 4.3.4a).

Further analyses of several of these cases are presented below.

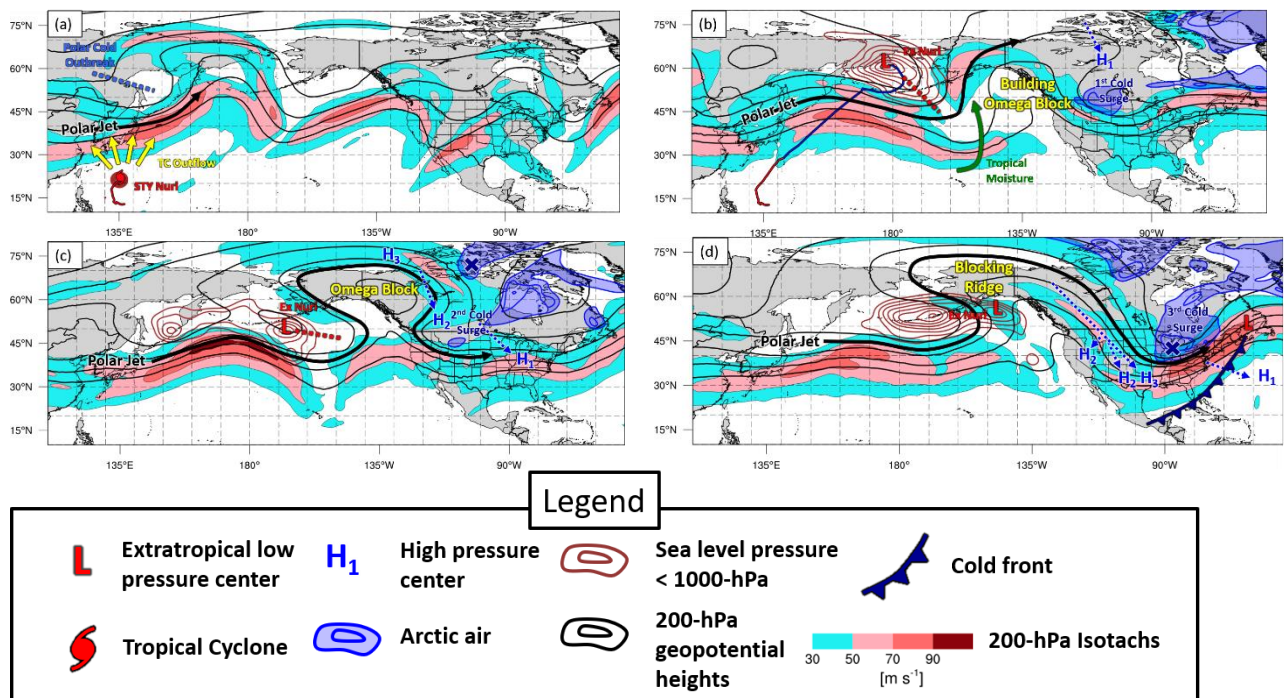


Fig. 4.3.3.5. 200 hPa geopotential height (black contours every 60 m), 200 hPa wind speed (color shading at 30, 50, 70, and 90 m s^{-1}), sea-level pressure (red contours every 4 hPa for values below 1000 hPa only), and subjectively identified Arctic air masses (blue shading), surface cyclones (red L), cold fronts, tropical cyclone (cyclone symbol), and surface anticyclones (blue H) at (a) 0000 UTC 4 November, (b) 1200 UTC 11 November, (c) 1200 UTC 15 November, and (d) 1200 UTC 18 November 2014. Figure adapted from Bosart et al. (2015a).

Super Typhoon Nuri (2014)

Nuri is notable for achieving a post-ET minimum sea-level pressure estimated at 924 hPa in the Bering Sea, which at least tied the record for the deepest extratropical cyclone observed over the North Pacific Ocean. Bosart et al. (2015a) show that prior to ET, Nuri's diabatically driven upper-tropospheric outflow helped to strengthen the north Pacific jet by increasing the meridional temperature gradient (Fig. 4.3.3.5a). Post-ET, diabatically driven outflow downstream of Nuri contributed to ridge building and omega block formation over northwestern Canada and eastern Alaska (Fig. 4.3.3.5b). This ridge building event and its subsequent evolution resulted in a deep upper-tropospheric trough developing over western and central North America, which led to three surges of cold, dry Arctic air into the United States over the subsequent week (Fig. 4.3.3.5c and d). In conjunction with these cold surges, 2,677 daily minimum temperature records were broken over the conterminous United States. Medium-range global numerical model guidance from NCEP failed to reliably forecast Nuri's downstream impact until 144 h prior to Nuri's peak extratropical intensity, and the 0-month NCEP Climate Prediction Center temperature forecast for the conterminous United States was nearly 180° out of phase from the verifying temperature pattern (not shown).

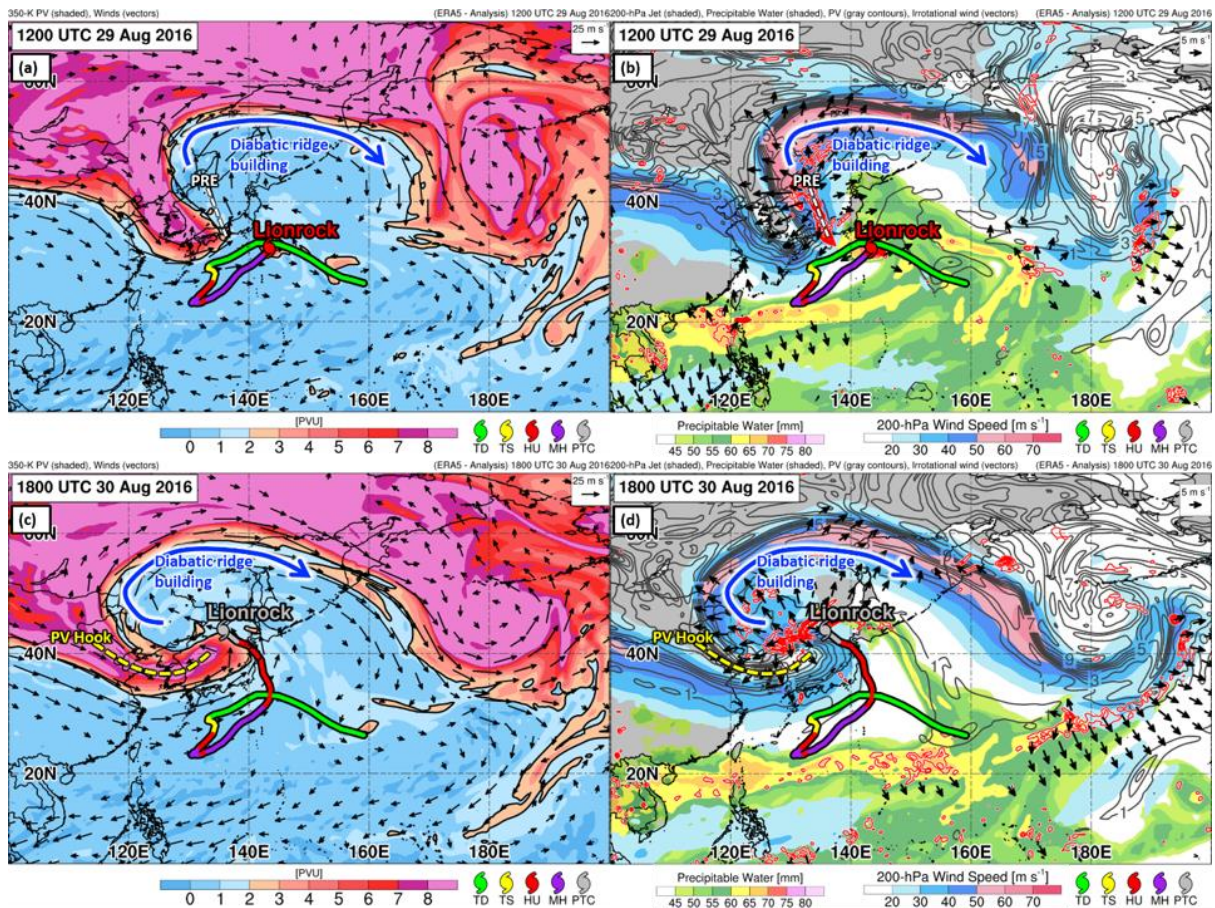


Fig. 4.3.3.6. (a) 350-K isentropic potential vorticity (PVU; shaded per the color bar) and horizontal wind (m s^{-1} ; reference vector at upper right) and (b) total precipitable water (mm; shaded per the left color bar), 200 hPa wind speed (shaded starting at 20 m s^{-1} per the right color bar), 250-150 hPa layer-mean potential vorticity (black contours every 1 PVU), 250-150 hPa layer-mean irrotational wind (m s^{-1} ; reference vector at upper right), and 600-400 hPa layer-mean ascent (red contours at values $< -5 \times 10^{-3} \text{ hPa s}^{-1}$) at 1200 UTC 29 August 2016. (c, d) As in (a, b), except at 1800 UTC 30 August 2016.

Typhoon Lionrock (2016)

Lionrock is notable for a series of binary and trinary interactions with other western North Pacific TCs that took place before the storm interacted with a strong early-season baroclinic trough and associated cyclone, underwent ET, triggered a strong PRE, and generated widespread flooding in northeastern Asia (Bosart et al. 2018). Diabatically driven ridge-building occurred with both Lionrock and its associated PRE (Fig. 4.3.3.6a). The orientation of the upper-tropospheric irrotational wind is consistent with frontogenetically forced ascent and diabatically driven ridge building due to negative PV advection (Fig. 4.3.3.6b). This pattern continues through Lionrock's ET as the upstream trough acquires a significant negative tilt (Fig. 4.3.3.6c and d). The upstream trough with which Lionrock interacted during its ET was highly anomalous for late

summer, exceeding -6 standard deviations for 500 hPa geopotential height at its core on 30 August (not shown).

4.3.4 Predictability and Predictions of Extratropical Transition

One of the ultimate goals of ET research is to improve our ability to predict the transition of TCs and their effects on the midlatitude flow, most notably those related to downstream high-impact weather events. In this context, it is important to distinguish between predictability (the intrinsic uncertainty in the system) and predictions (our ability to forecast an event), noting that predictability establishes an upper limit on our deterministic predictive skill (Melhauser and Zhang 2012). Studies of intrinsic predictability rely heavily on the combination of analysis, modeling and observational data sources, while those related to predictive skill often focus more directly on guidance, forecasts from RSMCs, and the optimal use of observations in data assimilation systems. Recent investigations of all of these elements that contribute to the forecasting challenges associated with ET will be discussed in this section.

a) Intrinsic Predictability of ET

Numerous earlier studies have shown that the phasing between the upstream trough and the recurving TC has a dramatic impact on ET and the downstream impacts thereof [see Jones et al. (2003) for a review]. However, more recent work has highlighted the fact that other midlatitude features can also have an important impact on the predictability of downstream flow evolution. The climatological analysis of TCs interacting with nearly straight zonal jets by Riboldi et al. (2018) reveals that Rossby wave initiation is more likely to occur during ET in the presence of weak jets. This is because stronger jets prevent significant ridge building through the downstream advection of the PV anomalies produced during TC-jet interaction. Furthermore, Torn and Hakim (2015) suggest that reduced predictability following ET might be the result of ET generating new waves rather than amplifying existing waves that can be sampled by upstream observations. This argument agrees with recent findings of enhanced predictability associated with long-lived Rossby wave packets (Grazzini and Vitart 2015). Torn (2017) also demonstrated that elevated forecast spread emanates downstream from a transitioning TC regardless of whether there is an upstream wave packet. Because the downstream response to ET is primarily related to Rossby wave packets propagating along the midlatitude waveguide (Wirth et al. 2018), these studies suggest that uncertainties associated with the initiation of wave packets during ET can lead to the growth of downstream forecast errors even in the absence of phasing uncertainties with the upstream trough.

Partly as a result of such studies documenting the importance of basin scale cyclone-waveguide interactions, the North Atlantic Waveguide and Downstream Impact Experiment (NAWDEX) field campaign was designed to explore the impact of processes that disturb the jet stream, including ET, and their impact on downstream high-impact weather (Schäfler et al. 2018). The campaign's intensive observing period (IOP) took place from mid-September to mid-October 2016, over which time numerous extratropical and tropical cyclones were sampled. The overall conditions were quite favorable for investigations of diabatic heating, cyclone and jet stream interactions over the North Atlantic. Four research aircraft were used during NAWDEX, each equipped

with state-of-the-science remote-sensing and *in situ* instruments, along with numerous ground-based measurements. In all, the aircraft carried out 49 NAWDEX flight missions.

Of the six tropical cyclones that were sampled during the NAWDEX IOP, three underwent ET: Ian, Karl and Nicole. Despite Karl’s minimal intensity as a TC, the observational dataset for this storm is particularly unique because coordination with NOAA’s tropically focused Sensing Hazards with Operational Unmanned Technology field campaign (Dunion et al. 2018) meant that Karl and its large-scale environment were heavily sampled throughout the cyclone’s life cycle. Schäfler et al. (2018) highlight the key stages of the Tropical Storm Karl ET event: i) an upstream trigger, in this case TS Karl, ii) the dynamical interaction of ex-Karl with the jet stream, iii) downstream evolution of the ex-Karl disturbance, and iv) subsequent high-impact weather over Europe. In the Karl case, the 5-day forecasts exhibited relatively low predictability (Fig. 4.3.4.1).

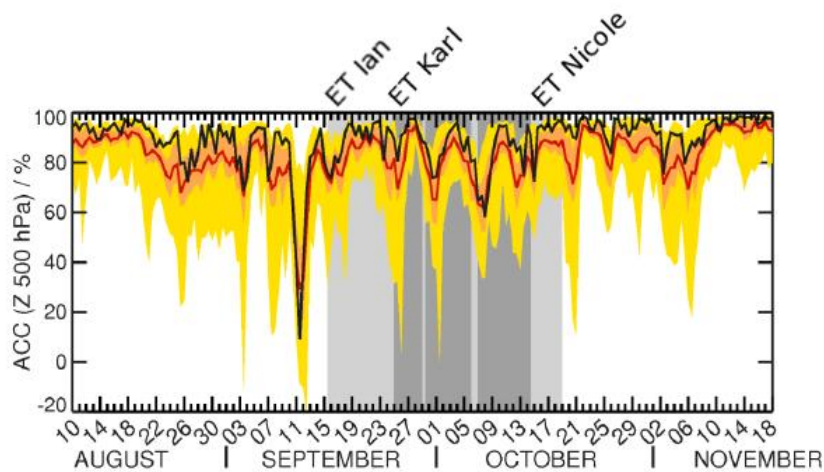


Fig. 4.3.4.1. Time series of the anomaly correlation of day-5 guidance from ECMWF for 500 hPa geopotential over an area from 35°N to 75°N and from 60°W to 0° (shown at the initial time of the forecast). The deterministic model is shown with the black line, the ensemble-mean with a red line, 50% of ensemble members with an orange line, and all ensemble member with yellow shading. The grey boxes represent weather regimes as described by Schafler et al. (2018). Individual ET events are noted at the top of the plot. Adapted from Schafler et al. (2018).

While NAWDEX took a broad view of basin-scale features and processes that limit predictability, the Hydrological cycle in Mediterranean eXperiment (HyMeX) field campaign focused on the eastern North Atlantic where the bulk of downstream high-impact weather associated with ET is expected to occur. The local dynamics and the predictability of such events at short range were investigated during the HyMeX first Special Observation Period (SOP1) in autumn 2012 (Drobinski et al., 2014; Ducrocq et al., 2014). Despite the clear dynamical linkage and consistent seasonality (Pinto et al. 2001), few studies have directly addressed the connections between ET, reduced predictability in the Mediterranean sector, and high-impact weather events.

The gap in our understanding of downstream North Atlantic ET impacts and associated predictability issues motivated Pantillon et al. (2015) to investigate the link

between tropical cyclones and Mediterranean weather during HyMeX SOP1. The authors performed five-day simulations of hurricanes Leslie, Rafael and Sandy with the Meso NH model in a domain encompassing the North Atlantic and the Mediterranean. Control simulations were compared to simulations in which the hurricanes were filtered out from the initial conditions. Pantillon et al. (2015) conclude that there is large case-to-case variability in downstream high impact weather (section 4.3.3b), but suggest that the interaction of tropical cyclones with the midlatitude flow over the western North Atlantic may be considered a perturbation to, rather than a source of, downstream wave breaking. These findings are also indicative of the fact that more research is needed to identify systematic differences between ET cases that amplify the downstream wave pattern and induce extreme weather and those that do not.

Although the HyMeX and NAWDEX field campaigns provide valuable observational evidence of the complex processes and interactions that limit predictability during ET and its potential downstream impacts, the necessarily restricted coverage of IOPs means that much of the resulting research focuses on a limited number of case studies. In an effort to place such studies in a broader context, recent research has adopted ensemble techniques to establish forecast climatologies that facilitate the comparison of downstream forecast uncertainty during ET to typical forecast spread for that time of the year. On average, recurving TCs are associated with comparatively higher forecast standard deviation, with cases in the western North Pacific cases being the least predictable (Ayyer 2015; Quinting and Jones 2016; Torn 2017). The region of enhanced standard deviation originates from where the TC enters the midlatitudes and spreads downstream at the Rossby wave group velocity. However, enhanced forecast uncertainty remains confined to the region of the transitioning TC in the absence of downstream development, highlighting the importance of Rossby wave packets to downstream forecast uncertainty (Fig. 4.3.4.2). With a reduction of the forecast skill horizon of approximately two days (Grams et al. 2015), predictability problems associated with ET appear to be larger than those related to baroclinic cyclones that occur in the same region during both winter and autumn seasons (Torn 2017).

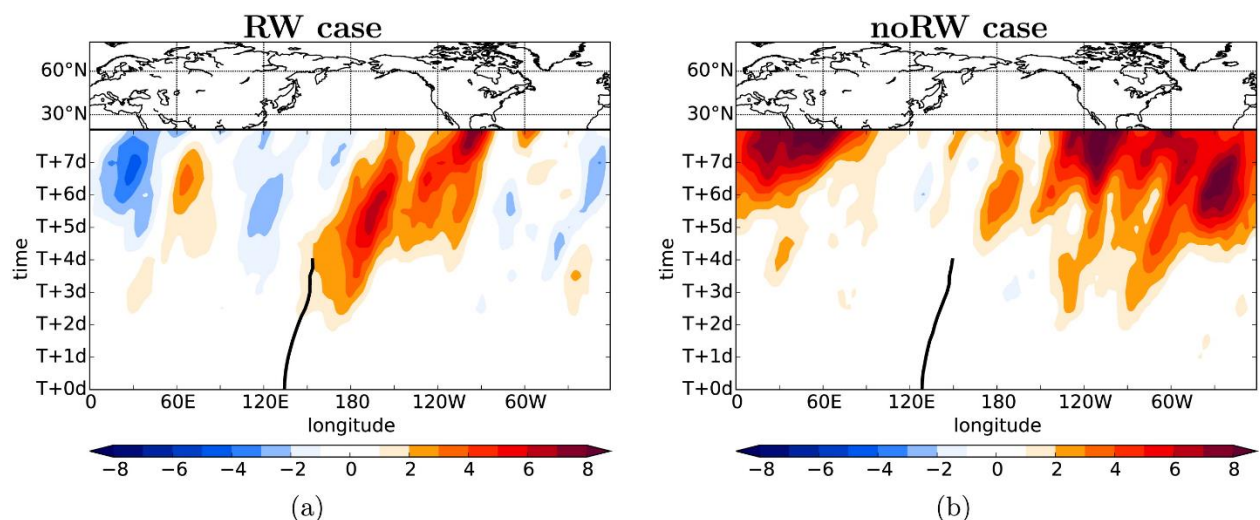


Fig. 4.3.4.2. Recurvature-relative composites of the anomaly of 250-hPa geopotential height ensemble standard deviation (shading, gpm) averaged between 20°N and 80°N

relative to June-November climatology for western north Pacific ET cases (a) with and (b) without downstream Rossby wave packets. Black thick line indicates the mean recurving track. From Quinting and Jones (2016).

Although universally applicable statements about the intrinsic predictability of ET remain elusive, the combination of climatological, modeling, observational and ensemble strategies have yielded important improvements in our understanding of the key processes and features that occur before, during and after ET. Such insights help us to assess the predictability of the ET process, particularly with regard to downstream high impact weather. This intrinsic predictability appears to be more limited than that of any of the individual components because the complex interactions between the “key ingredients” of ET occur over a broad range of spatial and temporal scales.

b) Assessing Predictability Limits: ET Sensitivity

The predictability of ET and its associated downstream impacts is naturally limited by the sensitivity of the features involved in the ET process to small perturbations. These initial seeds of uncertainty may develop on relatively small scales, but grow rapidly in sensitive regions during ET to affect both the environment in which the transition is occurring and the structure of the remnant TC itself.

i) Environmental Sensitivity

Cases and scenarios with large forecast errors during ET have motivated a number of recent modeling investigations, many of which focused on the transition, landfall, and downstream impacts of Hurricane Sandy (2012). Studies underscored strong sensitivity in track and ET timing (Munsell and Zhang 2014), and in the downstream midlatitude ridge amplification influenced by diabatic processes (Torn et al. 2015). Several studies have also highlighted the sensitivity of Sandy’s forecast tracks to the model configuration itself (Bassill 2014; Magnusson et al. 2014). In cases of especially high forecast sensitivity, such as Sandy, multiple factors often influence the forecast. In some cases, large sensitivity is associated with a bifurcation (Scheck et al. 2011) that occurs when a small change in one interaction parameter (e.g., midlatitude trough or TC vortex structure) results in a significant change in the storm’s track during transition. Bifurcation points are associated with the regions of strong deformation that can arise when the local relative velocity is zero, often in the base of a trough or along the apex of a ridge [see Riemer and Jones (2014), their Fig. 11]. As a TC approaches, the bifurcation point influences the likelihood of recurvature and eventual ET, as well as reduced the predictability of its post-transition outcome (Grams et al. 2013b; Riemer and Jones 2014; Keller et al. 2019).

Another example of a transitioning TC whose track was highly sensitive to the presence of such a structure in the environmental flow was Hurricane Nadine (2012), a storm that was also notable for its large forecast uncertainty (Munsell et al. 2015). Operational ensemble forecasts showed a bifurcation in Nadine’s track, with a significant fraction of members predicting landfall over the Iberian Peninsula, and large spread in the synoptic conditions downstream. This limited predictability was not only a major issue for planning observations during HyMeX SOP1, but also for modeling Nadine’s evolution and of the synoptic conditions over the Mediterranean in numerical experiments (Pantillon et al. 2015). Pantillon et al. (2016) clustered the ECMWF

ensemble forecast into two scenarios for interaction between Nadine and an Atlantic cut-off low, which controlled both the track of Nadine and the synoptic conditions downstream. The forecast bifurcation appears to have been related to the strength of the interaction between the transitioning TC and the cut-off low, with weaker interactions leading a westerly cyclone track and stronger interactions leading to a higher potential for landfall on the Iberian Peninsula (Fig. 4.3.4.3). Pantillon et al. (2016) found that the high forecast sensitivity to this vortex–vortex interaction resulted in the lowest predictability over the Mediterranean observed during HyMeX SOP1.

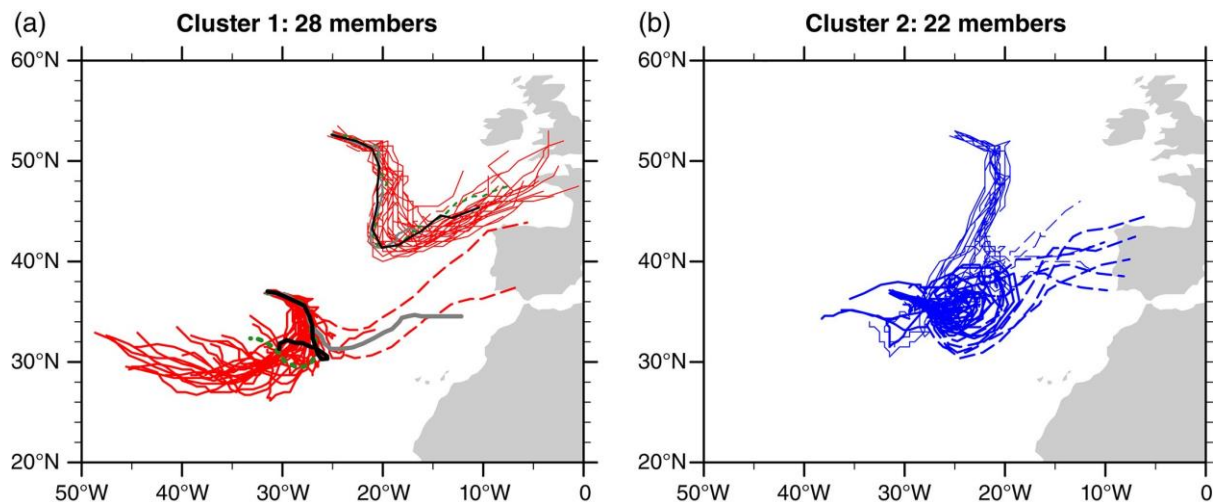


Fig. 4.3.4.3. Scenarios of (a) weak and (b) strong interaction between Hurricane Nadine and a cut-off low. Tracks of Nadine (thick curves) and the cut-off low (thin curves) in ECMWF ensemble members from 20 through 25 September 2012. The ECMWF analysis (black curve), deterministic forecast (grey curve) and control forecast (green curve) are also marked in (a). From Pantillon et al. (2016).

In order to assess such sensitivity to the environment in which ET is occurring, new ensemble-based diagnostic frameworks have been used to quantify uncertainty associated with the near-ET state and upstream features. In the case of Typhoon Choi-Wan (2009), Keller et al. (2014), and Keller (2017) identify different forecast scenarios using clustering techniques. They show that the different scenarios are associated with different rates of baroclinic energy conversion as the system undergoes ET (particularly to the east of the surface cyclone), leading to varying intensities of downstream waveguide amplification. Most of their sensitivity targets relate to the confluence region between the TC and the midlatitude trough immediately upstream. Other features further upstream of ET were found to be less important to the downstream flow response. They conclude that this case appears to be very sensitive to how the TC-midlatitude interaction modulates energy conversion from the background flow.

The evolution of the downstream state can also be sensitive to the interaction between the TC and the midlatitude flow itself, including nearby upper-tropospheric cyclones (Pantillon et al. 2016). From a forecasting perspective, Grams et al. (2015) showed that initializing TCs in the incorrect position can degrade the skill of a 3-day forecast of the downstream 500-hPa anomaly correlation to that of an 8-day forecast when the TC is initialized in the correct position. This study also highlights the sensitivity

of the downstream response to ascending warm conveyor belts ahead of the transitioning TC. The importance of such features in amplifying the downstream flow pattern and limiting the downstream predictability following ET were also emphasized by Grams and Archambault (2016). As a consequence, it appears that downstream forecast variability associated with ET events is case-specific. It is therefore important to expand these types of analyses to a larger set of cases and to consider the potential utility of simplified or idealized frameworks. Such studies will help us to understand why some ET events are more sensitive to *in situ* baroclinic and diabatic processes, while others are particularly sensitive to how the TC remnant interacts with the midlatitude flow.

ii) Storm-Scale Sensitivity

Although environmental conditions play an important role in establishing the limits of predictability during ET, the TC cannot be considered a passive player in the transition process because of both the remnant cyclonic potential vorticity and the large envelope of warm, moist air that the cyclone transports to higher latitudes. Sensitivity to these structures was exemplified during Hurricane Sandy's transition, during which Torn et al. (2015) show that NCEP's global forecast variability was characterized by large sensitivity to the interaction between diabatic outflow from convection associated with Sandy and the waveguide to the northwest. This result suggests that ET position forecasts are not solely attributable to upstream features: the TC and its associated convection can have a significant impact on the subsequent ET evolution.

Recent studies have also used adjoint and related singular vector sensitivity diagnostics to identify phenomena that influence storm evolution during ET. An adjoint model (the transpose of the tangent linear forecast model) allows for the efficient calculation of the sensitivity of a particular forecast aspect, or response function, to changes in the initial state under the tangent linear assumption. The related singular vector analysis permits the identification of the fastest growing perturbations to a given forecast. Magnusson et al. (2014) perform an evaluation of the ECMWF forecasts of Hurricane Sandy as it underwent ET, including a singular vector sensitivity analysis. They calculate the leading singular vector optimized for 48-h forecast total perturbation energy inside a box centered on Sandy as it is approaching the US east coast (Fig. 4.3.4.3) on 25 October 2012. The initial singular vector structure indicates that the forecast of Sandy is most sensitive to the structure of the subtropical ridge to the north and northeast of the storm. Part of the evolved singular vector structure stretches to the northwest of Sandy and is associated with the TC outflow as it starts to interact with midlatitude flow. The singular vector results are consistent with the ensemble analysis that they performed in the same study, which also highlights the importance of the strength of the subtropical ridge in determining if Sandy would make landfall along the eastern United States seaboard.

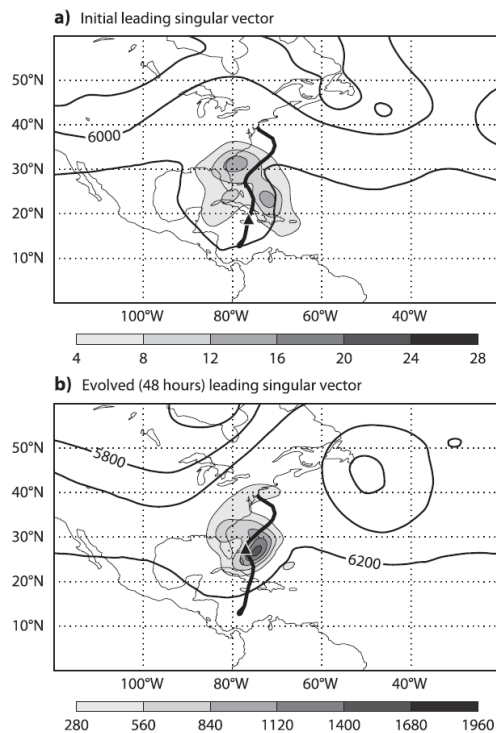


Fig. 4.3.4.3. Leading singular vector [(a) initial and (b) evolved] calculated for 0000 UTC 25 Oct (shaded) and targeted for Sandy after 48 h. Geopotential height averaged for 700, 500, and 300 hPa (thin contour lines) from the analysis at the valid time for the singular vector. The observed track (thick, black line) and position at the valid time for the singular vector (black triangle). From Magnusson et al. (2014), their Fig. 8.

Doyle et al. (2014) further examined the sensitivity of Hurricane Sandy near landfall using the Coupled Ocean/Atmosphere Mesoscale Prediction System (COAMPS®) moist adjoint. At short lead times, the forecast is most sensitive to moisture in the immediate vicinity of the TC and to vorticity in the area between the storm and the ridge to the north (Fig. 4.3.4.4). The sensitivity also extends towards the trough to the west, with some sensitivity associated with the low to the northeast. At longer lead times, the adjoint calculation indicates that the forecast was sensitive to the ridge directly to the north of the storm, the immediate upstream trough, as well as a mid-Pacific trough well upstream of the storm (not shown). These complex sensitivity patterns illustrate how the Sandy forecasts were sensitive to several different local and remote features, and shed light on why the forecast uncertainty for Sandy was so large.

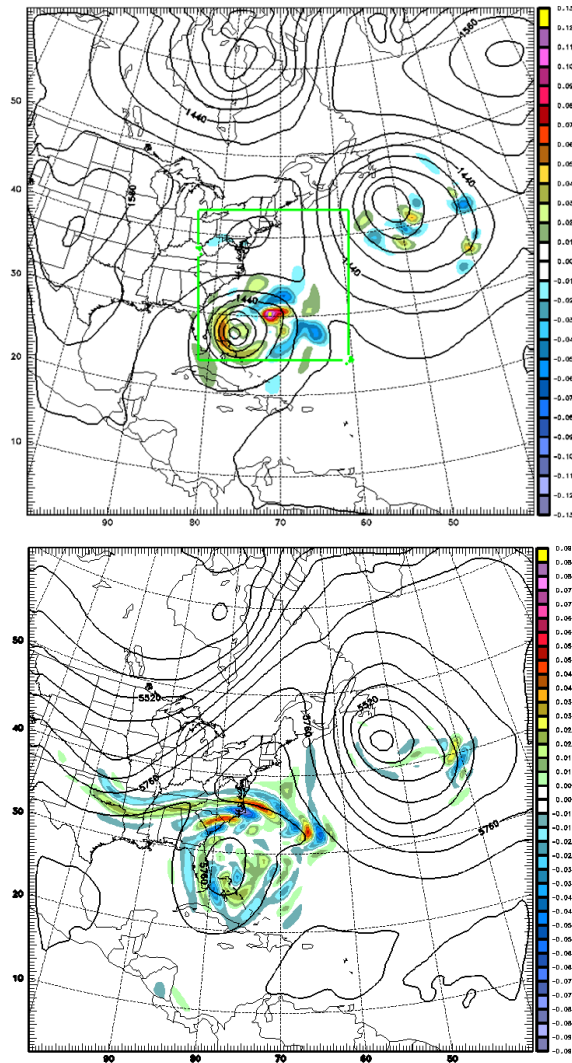


Fig. 4.3.4.4. The initial adjoint sensitivity from the 48-h 45-km COAMPS forecast initialized at 0000 UTC 27 October 2012. Left panel shows the analyzed 850-hPa heights (m), contours, and sensitivity to 850-hPa water vapor ($\text{m}^2 \text{s}^{-2} [\text{g kg}^{-1}]^{-1}$), shaded. Right panel shows analyzed 500-hPa heights (m), contours, and sensitivity to 500-hPa vorticity ($10^{-5} \text{m}^2 \text{s}^{-1}$), shaded. Adapted from Doyle et al. (2014).

Another COAMPS adjoint study, this one for Super Typhoon Lupit (2009), also finds highly complex sensitivity patterns during the ET. Reynolds et al. (2014) show that very short-range (12 h) forecast sensitivity to moisture extends from the area in the immediate vicinity of the storm along the developing frontal boundaries to the north and northeast of the storm (Fig. 4.3.4.5). They also found that the sensitivity patterns align with areas of strong frontogenesis and high PV. These adjoint results are complementary to ensemble-based tools and allow for quantitative identification of the processes and phenomena that influence storm evolution during ET. Their consistency with the results of sensitivity studies of storms observed during the T-PARC field

campaign (section 4.3.2a) lends additional credibility to this analysis technique and demonstrates its potential utility for observation targeting.

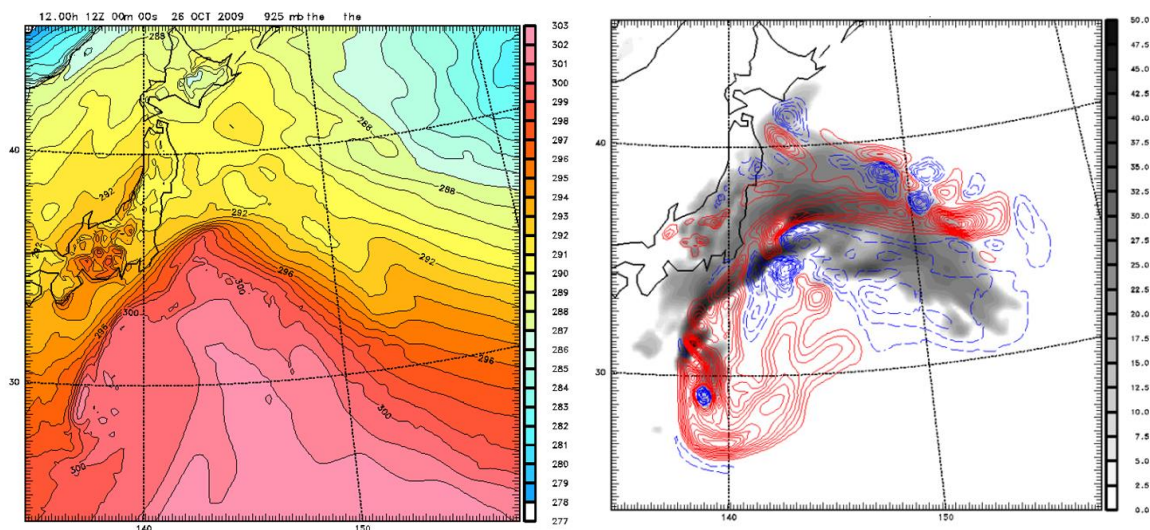


Fig. 4.3.4.5. The initial adjoint sensitivity from the 12-h 15-km COAMPS forecast initialized at 00Z 26 October 2009. Left panel shows the analyzed 925-hPa potential temperature (K). Left panels show the COAMPS simulated 925-hPa radar reflectivity (gray shading), and sensitivity to 850-hPa water vapor ($ci=0.05 \text{ m}^2 \text{ s}^{-2} [\text{g kg}^{-1}]^{-1}$), shaded. Adapted from Reynolds et al. (2014).

As a result of the observational relevancy of TC sensitive regions, NOAA undertook a concerted effort to use research aircraft to observe TCs undergoing ET without any direct influence from land as part of the Intensity Forecasting Experiment (Rogers et al. 2013). To date, five Atlantic TCs have been sampled [Hurricanes Earl (2010), Thomas (2010), Sandy (2012), and Arthur (2014) and Tropical Storm Karl (2016)] by multiple aircraft at multiple times during the transition period. The Karl observations are of particular interest because they dovetail with the NAWDEX basin-scale sampling described in section 4.3.4a. Additional NOAA aircraft missions that were conducted in the East Pacific sampled Hurricane Patricia (2015) during its encounter with a region of high baroclinicity over very warm water [with additional dropwindsonde observations from the Tropical Cyclone Intensity experiment (Doyle et al. 2017)]. Similar missions documented Hurricanes Dora (2011), Hilary (2011), and Simon (2014) as they encountered the cool sea surface in regions of high baroclinicity. Analyses of such datasets will help to evaluate the impacts of cool water and high baroclinicity on TCs, two elements to which the transition process appears to be particularly sensitive.

c) Practical Predictability of ET

The most direct measure of the current limits of practical predictability during ET is the quality of forecasts issued by operational centers before and during the event. It is this form of predictability, naturally limited by the intrinsic predictability described in section 4.3.4a and heavily influenced by the sensitivities discussed in section 4.3.4a, that has the largest direct effect on those who are affected by ET and its potential downstream impacts.

A linear discriminant analysis approach has been used to provide a climatological baseline TC classification to aid in the evaluation of operational and numerical model forecast skill (Aberson 2014). The predictors include position and intensity, as well as the 12-h trend of these two quantities and the current day of the year. Cyclone classification forecasts from NHC were found to be skillful at all lead times. However, ET forecasts could not be analyzed due to the small sample size, and as a result ET forecast skill relative to the baseline has yet to be quantified for forecasts from operational centers.

Recent improvements in deterministic and ensemble numerical guidance (e.g., Aberson et al. 2015; Zhang and Weng 2015; Weng and Zhang 2016), as well as observational capabilities, have benefited operational centers. An operational center's ET forecasts should be assessed within the context of expected numerical model forecast skill, including insight as to when skill is likely to be either anomalously high or low. An example of this is given by Sandy (2012), wherein members of the United States' global ensemble system with inaccurate track forecasts simultaneously had inaccurate cyclone classification forecasts (Kowaleski and Evans 2016).

Further intercomparison studies have focused on cases in which large disparities in guidance quality exist between operational centers. Key storm metrics computed by Magnusson et al. (2014), again for Hurricane Sandy (2012), illustrate such behavior (Fig. 4.3.4.6). Overall, the forecasts from ECMWF (gray dashed) are more consistent across initialization times. All ensembles show a positive bias (too weak) in the central pressure; however, the resolution of the forecasts in the TIGGE archive is inversely correlated with the central pressure bias (Davis 2018). All centers also underestimate the strength (maximum wind speed) of the cyclone. The CMC has the fastest-moving cyclones with too early landfalls, while ECMWF and UKMO have in general the slowest-moving cyclones.

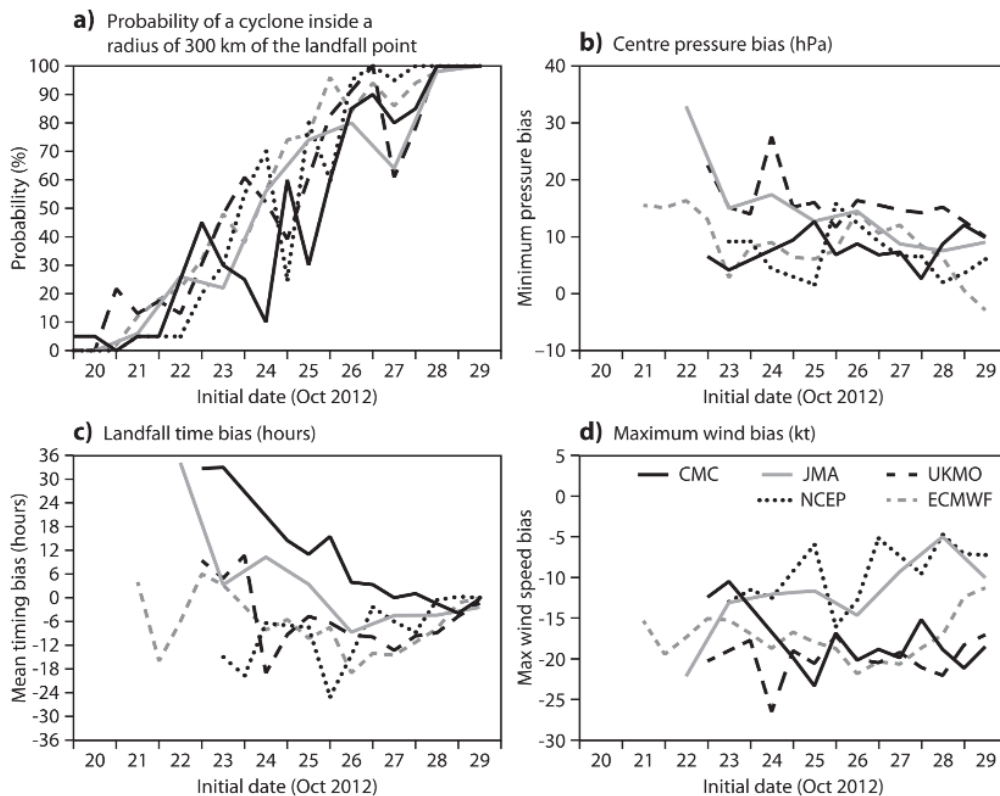


Fig. 4.3.4.6. Statistics for TIGGE ensemble forecasts from different initial times (x -axis). The ticks on the x -axis represent 0000 UTC. ECMWF (gray, dashed), UKMO (black, dashed), NCEP (black, dotted), CMC (black, solid), and JMA (gray, solid). Figure from Magnusson et al. (2014).

Using a larger sample of events, Leonardo and Colle (2017) verify 1-5 day multi-model ensemble forecasts of North Atlantic TCs verified against NHC's best tracks for the 2008-2015 seasons. They document an overall slow along-track bias, most of which occurs during the ET phase of the storm life cycle (Fig. 4.3.4.7). All models show a 25%-40% reduction in the slow bias when the extratropical phase of the storms is excluded from the evaluation. Guidance from the ECMWF shows the most significant improvement, with the magnitude of the day-5 along-track slow error decreasing from 200 km to 120 km when the ET cases are ignored. Leonardo and Colle (2017) note that the small sample size of ET cases prevents them from determining whether the improvements that they also observed over the 8-year study period were due to improved ET track forecasts, or to changes in the frequency of ET events.

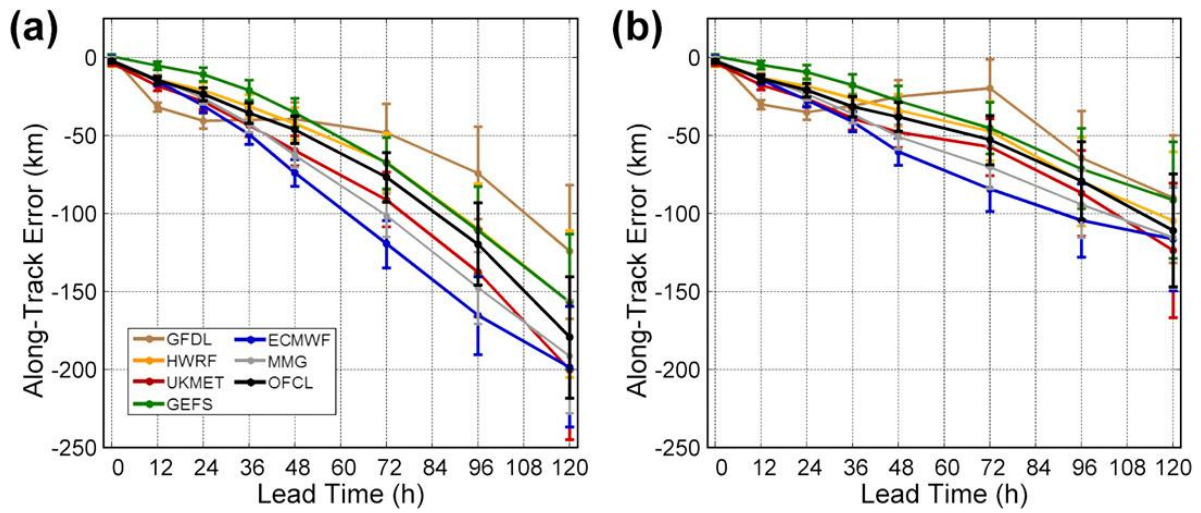


Fig. 4.3.4.7. Average 2008-2015 along track errors when (a) including and (b) excluding forecasts in which the observed TC was extratropical. Figure from Leonardo and Colle (2017).

4.3.5 Extratropical Transition and Climate

As long-period historical reanalyses become more available and the effects of climate change become increasingly felt by the general population, studies of ET in long-term contexts and under different climate-change scenarios have become more prevalent. These investigations help us to understand changes in the nature and frequency of ET over time, and to begin to assess current and future risks for vulnerable coastal populations.

a) Climatology of ET

One of the fundamental questions surrounding ET, and indeed TCs more generally, is whether there are any detectable trends in frequency-of-occurrence in the observational record. However, the relatively short length of the satellite era and the large interannual variability of ET frequency have made teasing out long-term trends in the historical record difficult. Mokhov et al. (2014) found a slightly positive trend in the fraction of TCs undergoing ET globally over the 1970-2012 period despite a slight decreasing trend in the North Atlantic. This result underscores the influence of large inter-basin differences on such analyses and suggests that more research efforts are required to identify secular trends in the ET record.

Considering all global basins, Bieli et al. (2018a,b) present an ET climatology from 1979 to 2017 using the Cyclone Phase Space [CPS; Hart (2003)], best-track and two reanalysis datasets (Fig. 4.3.5.1). They show that the basins with the highest fractions of ET are the North Atlantic and the western North Pacific (around 50%), and that the lowest relative frequency of occurrence is found in the eastern North Pacific and North Indian Ocean regions. The authors ascribe much of this inter-basin variability to the geography of the regions and to differences in mean steering flow. The western North Pacific and the North Atlantic are also the basins with the highest landfalling rates, followed by the Australian region. Bieli et al. (2018a,b) also note strong differences in seasonality between the basins. In the western North Pacific and the North Atlantic, storms are more likely to undergo ET late in the TC season. In contrast, the seasonal cycle in the Southern Hemisphere ET fraction is generally weak.

It is important to notice that the ET climatology is sensitive to the reanalysis used to calculate CPS, as well as the best-track dataset considered. ET fractions are higher when the CPS is calculated from the ERA-Interim reanalysis compared to the JRA-55 reanalysis (Fig. 5.1). Bieli et al. (2018b) suggest that JRA-55-derived CPS analyses better agree with best-track designations than do the corresponding ERA-Interim-derived analyses, with significant differences appearing in the eastern and central North Pacific regions. In these areas, the ERA-Interim reanalysis has a large number of false positives in which the CPS calculated using ERA-Interim fields suggests ET, but there is no ET label in the best-track dataset. Overall, ET classifications using CPS in both reanalysis datasets agree best with the best-track designations in the North Atlantic and western North Pacific basins, perhaps in part because the CPS is used operationally by the RSMCs in these regions. In contrast to Mokhov et al. (2014), Bieli et al. (2018a) did not find any statistically significant trends in ET fraction except in the South Indian Ocean.

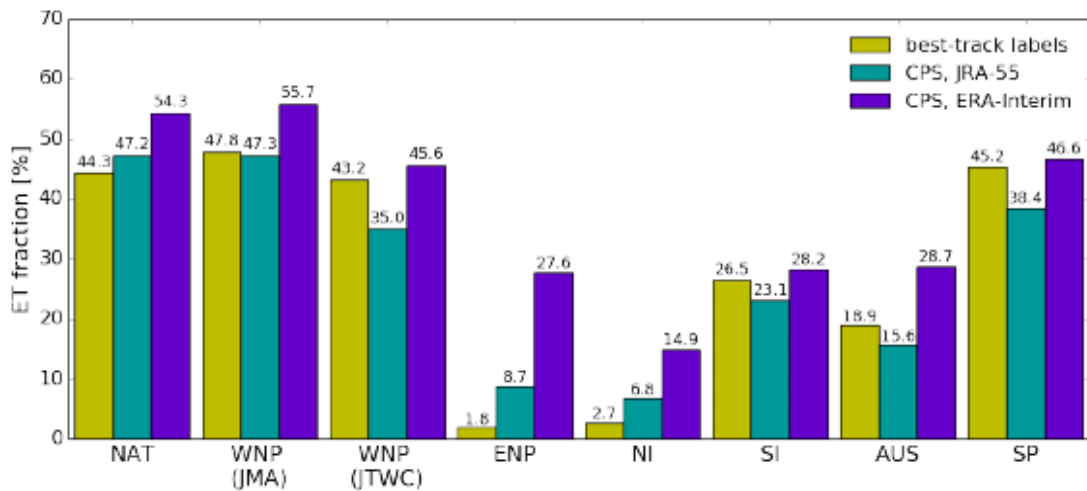


Fig. 4.3.5.1. Climatological percentage of TCs that undergo ET in each basin [North Atlantic (NAT), western North Pacific (WNP), eastern North Pacific (ENP), North Indian Ocean (NI), Australian region (AUS), South Pacific (SP)] as defined by the best-track labels and CPS using the JRA-55 and ERA-Interim reanalyses. Reproduced from Bieli et al. (2018a).

Such focused studies of the ET climatology remain rare, and much of our understanding of recent trends in TC-midlatitude interactions is gained indirectly from studies of the tropical phase of the TC life cycle. For example, Kossin et al. (2014) found an increase in the latitude of maximum intensity of TCs over the last 30 years, associated with a poleward shift in genesis locations (Daloz and Camargo 2018; Studholme and Gulev 2018; Sharmila and Walsh 2018), which is projected to continue (Kossin et al. 2016). Shaw et al. (2016) also highlight the uncertainty of predictions of the complex spatial patterns of baroclinicity and displacements in extratropical storm tracks. Predicted changes in these features appear to vary by both season and hemisphere, implying that changes in ET may be regional in nature.

b) Extratropical Transition in Climate Models

Despite the uncertainty in the recent historical record surrounding ET, projections of the frequency-of-occurrence and spatiotemporal characteristics of TC recurvature and ET are required by decision makers, insurers, and other groups that seek to understand and mitigate risks associated with ET. With issues in the length of the historical record and reporting biases such as those outlined in Landsea et al. (2010), high-resolution climate models have been used with increasing frequency to study TC-climate interactions (Walsh et al. 2015; Wehner et al. 2015; Camargo and Wing 2016; Yoshida et al. 2017). The current consensus projection is that globally, TCs will become less frequent but intense storms will become stronger (the tail of the intensity distribution is extended) with heavier precipitation (Knutson et al. 2010; Walsh et al. 2016). Despite the increasing volume of published literature regarding potential changes of TCs in an evolving climate, ET has received relatively little attention.

Recent efforts have been undertaken to apply traditional ET metrics [including the Hart (2003) CPS] to climate model output. Generally, TCs are handled in a Lagrangian, storm-following framework. However, with climate integrations, no observational track record exists, necessitating the need for objective, automated detection and tracking algorithms. TC climatology and projections are sensitive to the thresholds used in these tracking algorithms, especially for low-resolution models and weak TCs (Horn et al. 2014; Zarzycki and Ullrich 2017).

Notwithstanding this limitation, Liu et al. (2017) investigated North Atlantic ET events in high-resolution simulations from the Geophysical Fluid Dynamics Laboratory's Forecast-Oriented Low Ocean Resolution model that followed Representative Concentration Pathway 4.5 (RCP4.5) scenario protocols. They found that despite a decrease in TC frequency in the North Atlantic basin under RCP4.5, the number of storms undergoing ET increased slightly (Fig. 4.3.5.2). This results in a projected increase in the ET ratio that Liu et al. (2017) propose to be a response to the shifts in TC genesis described in section 4.3.5a. With a more favorable storm formation environment over the eastern North Atlantic, the preferred recurvature track lies in the western North Atlantic at the expense of storms forming and tracking into the Caribbean Sea and Gulf of Mexico. In a follow-up study using the same simulations, Liu et al. (2018) analyzed rainfall along the eastern United States seaboard associated with both ET and non-ET TC events. They found an increase in the rainfall associated with ET events in the northeastern United States due an increase in transitioning storm frequency, but prior to ET onset itself. It is important to note that these results are based on single-model studies and focused only on the North Atlantic basin. Multi-model studies targeting the global climatology of ET are needed to produce a more complete picture of ET in a changing climate.

A drawback of using the Hart (2003) CPS in a climate modeling context is that it requires output to be saved on multiple vertical levels with high temporal frequency. For long-term, high-resolution simulations completed over the past decade, many groups have opted for reduced output data streams at sub-daily timescales. Baatsen et al. (2015) develop a simplified ET algorithm that detects collocated equivalent potential temperature anomalies and potential vorticity centers associated with cyclones in the North Atlantic. They find that a warmer Atlantic Ocean decreases the duration of ET and results in an increased frequency of post-ET reintensification that has clear implications for Western Europe.

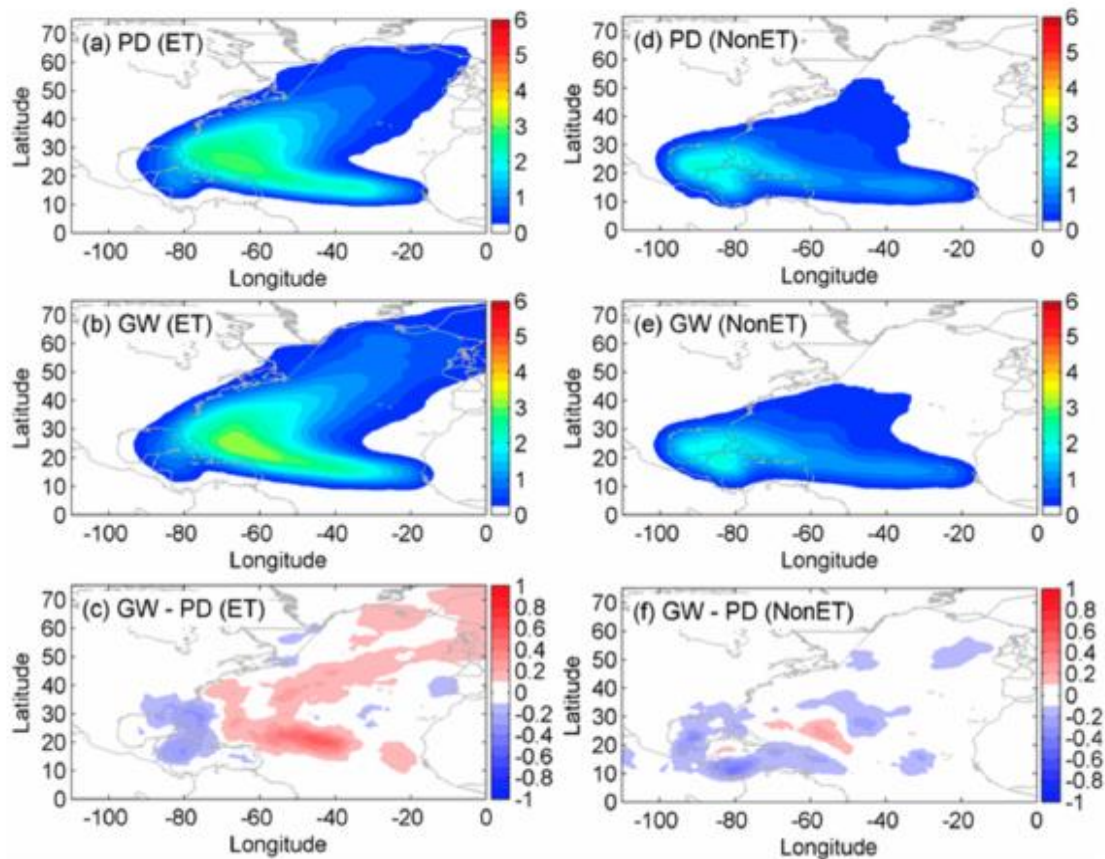


Fig. 4.3.5.2. The climatological TC density of storms undergoing ET events in (a) present-day and (b) RCP4.5 global warming simulations using GFDL FLOR. TC events not undergoing ET are shown in (d) and (e). The future change of annual TC density of ET and non-ET events are shown in (c) and (f). Reproduced from Liu et al. (2017).

Zarzycki et al. (2017) are able to apply the full CPS ET detection technique to high resolution simulations from the NCAR Community Atmospheric Model. They find systematic differences between the model results and diagnostics from the Climate Forecast System and ERA-Interim reanalyses for North Atlantic storms over the 1980-2002 period. The largest number of ET events occurs in September in both the model simulations and reanalyses; however, the month with the 2nd largest number of ET occurrences in the simulations is October, as opposed to July in the reanalyses and IBTrACS (Knapp et al. 2010). They also find that the ET process extends for a longer time period in the model simulations than in the reanalyses. While the simulations show ET onset at about the same latitude as the reanalyses, ET completion occurs further north and east in the model than in the reanalyses (Fig. 4.3.5.3). They further find that the simulations have a higher fraction of ET events following the “asymmetric then cold-core” pathway compared to the “cold-core then asymmetric” pathway than is found in the reanalyses. The “long” bias in ET duration is primarily tied to the former pathway bias. This implies that the modeled TCs take longer than analyzed to become cold-core

after becoming asymmetric, which the authors hypothesize may be due to differences in the mean flow or parameterized physical processes. In either case, biases in event duration suggest that there may be systematic structural errors present during ET in climate models, a finding that needs to be investigated in other modeling systems and basins before any general conclusions can be drawn.

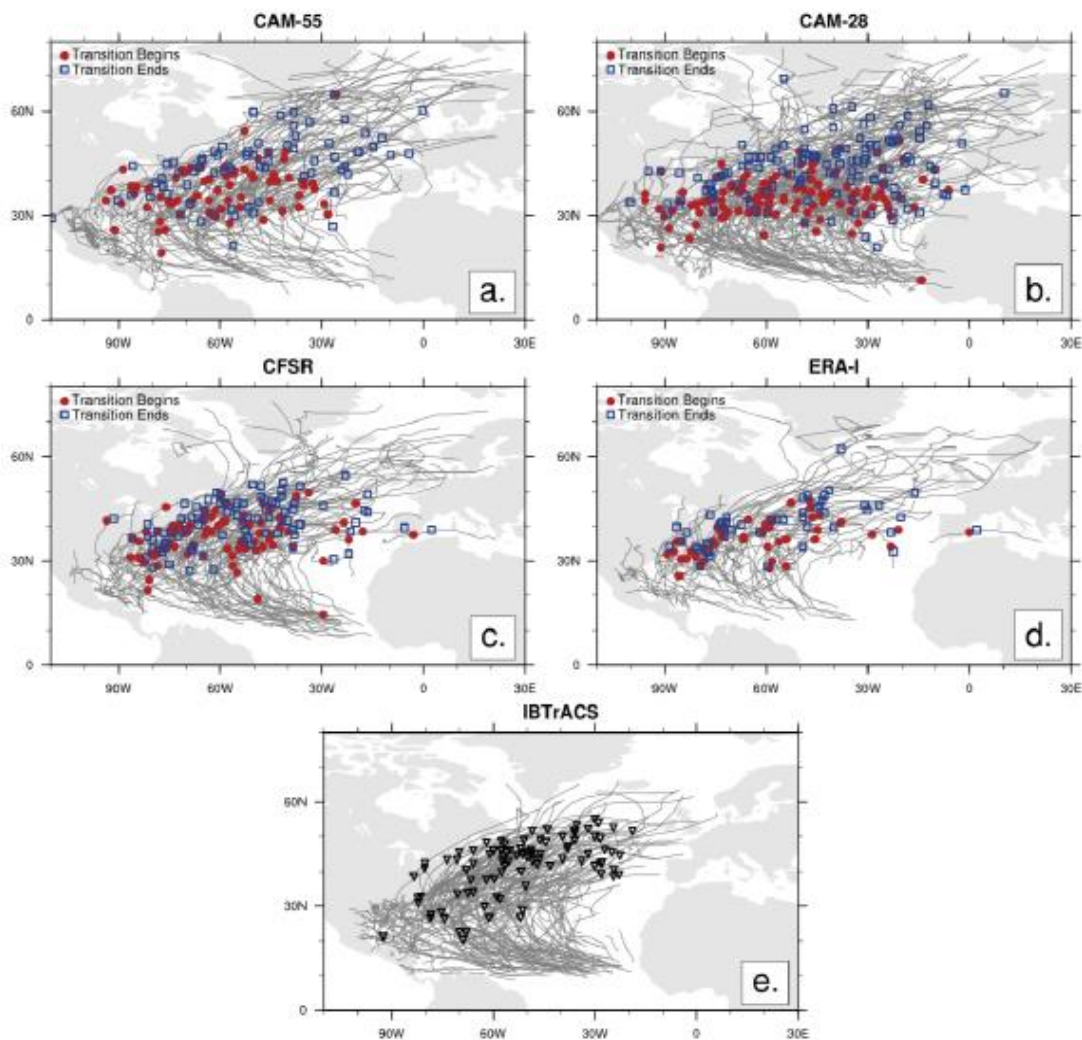


Fig. 4.3.5.3. Objectively tracked storm trajectories from 1980 to 2002 for (a) a 55 km version of the NCAR Community Atmospheric Model, (b) a 28 km version of the model, (c) the Climate Forecast Systems Reanalysis, and (d) the ERA-Interim reanalysis. In the panels (a) through (d), gray lines indicate the full trajectory from TC genesis to extratropical cyclone decay, red circles indicate the beginning of ET, and blue squares indicate the completion of ET. IBTrACS trajectories are shown in (e) with instantaneous ET being denoted by black triangles. Reproduced from Zarzycki et al. (2017).

c) Extratropical Transition Sensitivity to Climate Change

Another framework that has received attention recently for studying climate impacts on weather-scale phenomena is the application of background anthropogenic “fingerprints” to model simulations in a case-study context. Sometimes referred to as “detection and attribution” or “pseudo-global warming” configurations (Schär et al. 1996), these experiments seek to understand storm-level sensitivity to climate perturbations within a constrained synoptic setup.

Although pseudo-global warming work has primarily been focused on TCs [for example Knutson et al. (2008) and Wehner et al. (2018)], a few recent case studies in the North Atlantic have relevance to the ET community. Lackmann (2015) noted that, when using pre-1900 large-scale climate deltas, Hurricane Sandy became weaker and made landfall further south along the Eastern Seaboard (while undergoing ET) than observed. Conversely, when post-2100 climate increments were applied, Lackmann (2015) found that the storm was stronger and made landfall at a higher latitude. More recent work applying the pseudo-global warming framework to an idealized simulation of Hurricane Irene shows that super-Clausius–Clapeyron scaling of precipitation rates during ET may occur (due to increases in dynamical moisture convergence and surface fluxes), and that the duration of the transitioning phase may increase (Jung and Lackmann 2018). This extension of the transition period would permit tropical impacts to persist further poleward in a warming climate.

In one of the few ongoing pseudo-global warming projects that directly addresses the ET process, Michaelis and Lackmann (2018) have applied this framework to study ET changes using NCAR’s Model for Prediction Across Scales. It is clear that demand for information about the climate sensitivity of ET from decision makers and the general public will only increase over time, and that a concerted effort on the part of the ET research community is required to be able to respond with robust and general statements about this important subject.

4.3.6 Summary and Recommendations

Since the last IWTC four years ago, notable advances have been made in our understanding of ET, particularly as it relates to the collection of *in situ* observations of structural change, and indirect and downstream impacts from ET events. However, there remain many fruitful directions for future research, as posed in Evans et al. (2017) and Keller et al. (2019). These and other recommendations are synthesized here.

A universally applicable definition for extratropical transition does not exist, a fact that harms the community’s ability to make robust, general statements about both specific cases and the ET climatology. Although the cyclone phase space of Hart (2003) has become the *de facto* classification standard, it does not resolve the transitioning cyclone’s inner core, is reliant on model-derived analyses and forecasts, suffers from ambiguity with warm-seclusion events and requires information that may be difficult to obtain in a climate modeling context. A discussion is recommended as to whether a universally applicable alternative definition is necessary and achievable. Such a definition would prove particularly useful in developing an internally consistent global ET climatology and for comparisons between studies based on reanalysis data and climate model output.

Much of the research documented here and in Evans et al. (2017) and Keller et al. (2019) is primarily fundamental in nature. There have been few advances in operational/applied research as it relates to ET in recent years. Representative examples include the “no skill” model for cyclone phase classification of Aberson (2014) and a regression-based adjustment to the Advanced Dvorak Technique remote intensity estimation method based in part on Manion et al. (2015). Recent high-impact ET events such as North Atlantic TC Sandy (2012) highlight forecast communication issues during ET events, as discussed in the IWTC-8 report, and suggest that further work is needed to improve our ability to effectively communicate evolving cyclone threats during ET to the public. Further, recent advances in geostationary and polar-orbiting satellite technology enable us to observe transitioning cyclones better than ever before, and suggest that further research on how to best leverage these technologies in the advisory and forecast (both operational and numerical) process is warranted. The optimal use of such observations also involves data assimilation systems, an important component of the forecasting system that has received relatively little ET-focused attention in recent years.

Although recent years have seen the collection of the first *in situ* observations of structural change during ET, the sample size of cyclones for which such observations exist is very small, and more observations are necessary to document and understand case-to-case variability. This also applies to the direct impacts (wind, waves, and rainfall) that accompany ET, downstream development, and other indirect impacts of ET events including downstream high impact weather events. Detailed analyses of data from the recent NAWDEX, HyMeX and NOAA sampling campaigns may prove fruitful in these regards.

Data from these field campaigns are already being used in process studies that will help to quantify the intrinsic predictability of ET by identifying sources of sensitivity and documenting the complex interactions between the features involved in the transition. The combination of such investigations with ensemble- and adjoint-based methods for estimating predictability will help to estimate an upper bound for potential forecast improvements. Approaching this problem simultaneously from multiple directions is particularly useful because the detailed data from field campaigns are necessarily limited to a small number of cases, while the modeling and analysis frameworks can be extended to larger sample sizes. The natural extension of these studies into investigations of practical predictability mandates the use of such larger datasets because of the relatively small number of ET events annually and large case-to-case variability. Accordingly, the increased use of ensemble reforecast datasets for studies of forecast skill may help to establish a baseline for the practical predictability of ET in current numerical guidance.

Research conducted over a decade ago (Hart et al. 2006) documented the conditions under which transitioning TCs would decay or intensify post-ET; however, the sample sizes for each set of cases were very small, and post-ET intensity change remains a forecast challenge. For example, earlier studies (e.g., Hart et al. 2006; McTaggart-Cowan et al. 2007; Pantillon et al. 2013) suggest that intensification is generally associated with a negatively upstream tilted middle-tropospheric trough and associated strong middle tropospheric cyclone vorticity advection over the TC. Though this is generally thought of as a first-order qualitative influence on extratropical cyclone intensity, crucial details of this process remain to be quantified and warrant further investigation.

Significant advances in understanding of the downstream impacts of recurring TCs have been made in recent years, particularly for the western north Pacific and Atlantic basins. However, most studies have emphasized individual case studies, with comparatively few studies (e.g., Grams and Archambault 2016; Archambault et al. 2013, 2015) focusing on climatological or composite analyses. The systematic investigation of linkages between ET events in all basins and downstream high-impact weather constitutes an intriguing research opportunity, whether for individual basins or in comparing differences between basins (e.g., such as may arise due to different climatological states of the midlatitude waveguide between the western north Pacific and Atlantic). Further, the idea that a transitioning TC may indirectly precondition the midlatitude waveguide (e.g., through a PRE) and thus impact their subsequent interaction and downstream response is relatively recent, and further investigation is recommended to quantify the extent to which preconditioning occurs and its attendant impacts to the downstream response and hemispheric-scale predictability. Finally, most downstream development studies have focused on the synoptic scales. Preliminary research suggests that some ET events may have impacts extending to the sub-seasonal to seasonal scales, and further study is warranted to document these impacts, better understand the underlying physics and dynamics, and quantify the predictability changes associated with such events.

At even longer time scales, recent years have seen the publication of the first studies with the goal of document or predicting the influence of climate change on ET climatologies and impacts, particularly in downstream regions. Given the apparent presence of persistent differences between reanalysis datasets and systematic model errors during ET, more studies in this vein are required to allow the community to make clear and compelling statements about the presence or absence of secular trends in ET in both the historical record and in climate projections. Such an effort is also required in the realm of attribution studies, not the least to assess whether current “fingerprint” technique is reliable for such studies given the complex dynamical interactions involved in the ET process. One thing that is certain about this emerging component of the ET field is that the results of these studies will be of significant interest to decision makers and the general public both in regions that currently experience ET and in those that are predicted to begin to feel the effects of transitioning storms in the future.

Table of Acronyms

<u>Acronym</u>	<u>Expansion</u>
CMC	Canadian Meteorological Centre
COAMPS	Coupled Ocean/Atmosphere Mesoscale Prediction System
CPS	Cyclone phase space
ECMWF	European Centre for Medium-Range Weather Forecasts
ERA-Interim	ECMWF Interim reanalysis
ET	Extratropical transition
HyMeX	HYdrological cycles in the Mediterranean Experiment
IBTrACS	International Best Track Archive for Climate Stewardship
IOP	Intensive Observing Period
JMA	Japanese Meteorological Agency
NAWDEX	North Atlantic Waveguide and Downstream impact EXperiment
NCAR	National Center for Atmospheric Research
NCEP	National Centers for Environmental Prediction
NHC	National Hurricane Center
NOAA	National Oceanographic and Atmospheric Administration
PRE	Precedessor rain event
PV	Potential vorticity
PVU	Potential vorticity unit
RSMC	Regional Specialized Meteorological Centre
RWP	Rosby wave packet
SOP	Special Observing Period
TC	Tropical cyclone
THORPEX	THE Observing system Research and Predictability EXperiment
TIGGE	THORPEX Interactive Grand Global Ensemble
T-PARC	THORPEX Pacific-Asian Regional Campaign
UKMO	United Kingdom Met Office

References

- Aberson, S. D., 2014: A climatological baseline for assessing the skill of tropical cyclone phase forecasts. *Wea. Forecasting*, **29**, 122–129.
- Aberson, S. D., A. Aksoy, K. J. Sellwood, T. Vukicevic, and X. Zhang, 2015: Assimilation of high-resolution tropical cyclone observations with an ensemble Kalman filter using HEDAS: Evaluation of 2008–11 HWRF forecasts. *Mon. Wea. Rev.*, **143**, 511–523.
- Agusti-Panareda, A., C. D. Thorncroft, G. C. Craig, and S. L. Gray, 2004: The extratropical transition of hurricane Irene (1999): A potential-vorticity perspective. *Quart. J. Roy. Meteor. Soc.*, **130**, 1047–1074.
- Aiyyer, A., 2015: Recurving western North Pacific tropical cyclones and midlatitude predictability. *Geophys. Res. Lett.*, **42**, 7799–7807.
- Anwender, D., P. A. Harr, and S. C. Jones, 2008: Predictability associated with the downstream impacts of the extratropical transition of tropical cyclones: Case studies. *Mon. Wea. Rev.*, **136**, 3226–3247.
- Archambault, H. M., L. F. Bosart, D. Keyser, and J. M. Cordeira, 2013: A climatological analysis of the extratropical flow response to recurving western North Pacific tropical cyclones. *Mon. Wea. Rev.*, **141**, 2325–2346.
- Archambault, H. M., D. Keyser, L. F. Bosart, C. A. Davis, and J. M. Cordeira, 2015: A composite perspective of the extratropical flow response to recurving western north Pacific tropical cyclones. *Mon. Wea. Rev.*, **143**, 1122–1141.
- Atallah, E. H., L. F. Bosart, and A. R. Aiyyer, 2007: Precipitation distribution associated with landfalling tropical cyclones over the eastern United States. *Mon. Wea. Rev.*, **135**, 2185–2206.
- Baatsen, M., R. J. Haarsma, A. J. Van Delden, and H. de Vries, 2015: Severe autumn storms in future Western Europe with a warmer Atlantic Ocean. *Clim. Dyn.*, **45**, 949–964.
- Baek, E. H., G. H. Lim, J. H. Kim, and J. S. Kug, 2015: Antecedent mid-tropospheric frontogenesis caused by the interaction between a tropical cyclone and midlatitude trough: a case study of Typhoon Rusa (2002). *Tellus*, **67**, 27476.
- Bassill, N., 2014: Accuracy of early GFS and ECMWF Sandy (2012) track forecasts: Evidence for a dependence on cumulus parameterization. *Geophys. Res. Lett.*, **41**, 3274–3281.
- Bieli, M., S. J. Camargo, A. H. Sobel, J. Evans, and T. M. Hall, 2018a: A global climatology of extratropical transition. Part I: Characteristics across basins. *J. Climate*, in review.
- Bieli, M., S. J. Camargo, A. H. Sobel, J. Evans, and T. M. Hall, 2018b: A global climatology of extratropical transition. Part II: Statistical performance of the cyclone phase space. *J. Climate*, in review.

- Black, M. L., J. F. Gamache, F. D. Marks, C. E. Samsury, and H. E. Willoughby, 2002: Eastern Pacific Hurricanes Jimena of 1991 and Olivia of 1994: The effect of vertical shear on structure and intensity. *Mon. Wea. Rev.*, **130**, 2291–2312.
- Bosart, L. F., D. Keyser and A. C. Winters, 2015a: An investigation of the skill of week-two extreme temperature and precipitation forecasts at the NCEP-WPC. Presentation at the *NGGPS Annual Meeting and External FFO PI Meeting*, College Park, MD, USA.
- Bosart, L. F., B. J. Moore, J. M. Cordeira, and H. M. Archambault, 2017: Interactions of north Pacific tropical, midlatitude, and polar disturbances resulting in linked extreme weather events over North America in October 2007. *Mon. Wea. Rev.*, **145**, 1245–1273.
- Bosart, L. F., P. P. Papin, A. M. Bentley and T. Burg, 2018: TC Lionrock (2016) Touches All the Bases during Its Lifecycle: Monsoon Gyre, Tropical Transition, TC-TC Interactions, a Predecessor Rain Event, and Extratropical Transition. Abstract, 33rd *Conference on Hurricanes and Tropical Meteorology*. Ponte Verda, FL, USA.
- Bosart, L. F., P. P. Papin, A. M. Bentley, B. J. Moore, and A. C. Winters, 2015b: Large-scale antecedent conditions associated with 2014–2015 winter onset over North America and mid-winter storminess along the North Atlantic coast. Abstract, 17th *Cyclone Workshop*, Pacific Grove, CA, USA.
- Bruneau, N., J. Grieser, T. Loridan, E. Bellone, and S. Khare, 2017: The impact of extra-tropical transitioning on storm surge and waves in catastrophe risk modelling: Application to the Japanese coastline. *Nat. Hazards*, **85**, 649–667.
- Camargo, S. J., and A. A. Wing, 2016: Tropical cyclones in climate models. *WIREs Clim. Change*, **7**, 211–237.
- Chen, H. 2015: Downstream development of baroclinic waves in the midlatitude jet induced by extratropical transition: A case study. *Adv. Atmos. Sci.*, **32**, 528–540.
- Chen, H., K. Wang, J. M. Wang, X. T. Zhang, Y. F. Wang, and W. L. Wang, 2017: A case study on the sensitivity of downstream development to typhoon intensity and its initial location. *Met. Apps.*, **24**, 444–456.
- Corbosiero, K. L., and J. Molinari, 2002: The effects of vertical wind shear on the distribution of convection in tropical cyclones. *Mon. Wea. Rev.*, **130**, 2110–2123.
- Cordeira, J.M., N.D. Metz, M.E. Howarth, and T.J. Galarnau, 2017: Multiscale upstream and in situ precursors to the elevated mixed layer and high-impact weather over the midwest United States. *Wea. Forecasting*, **32**, 905–923.
- Daloz, A. S., and S. J. Camargo, 2018: Is the poleward migration of tropical cyclone maximum intensity associated with a poleward migration of tropical cyclone genesis? *Clim. Dyn.*, **50**, 705–715.
- Davis, C. A., 2018: Resolving tropical cyclone intensity in models. *Geophys. Res. Lett.*, **45**, 2082–2087.

- DeHart, J. C., R. A. Houze Jr., and R. F. Rogers, 2014: Quadrant distribution of tropical cyclone inner-core kinematics in relation to environmental shear. *J. Atmos. Sci.*, **71**, 2713–2732.
- Deng, D. and E. A. Ritchie, 2018a: Rainfall characteristics of recurving tropical cyclones over the western north Pacific. *J. Climate*, **31**, 575–592.
- Deng, D. and E. A. Ritchie, 2018b: A metric for rainfall asymmetry in recurving tropical cyclones. *Geophys. Res. Lett.*, **45**, 6741–6749.
- Doyle, J. D., R. Langland, P. A. Reinecke, C. Amerault, 2014: Multi-scale Predictability Aspects of Superstorm Sandy. Presented at Superstorm Sandy and the Built Environment: New Perspectives, Opportunities, and Tools, Atlanta, GA, 2-6 February 2014. Abstract and link to recorded presentation available at <https://ams.confex.com/ams/94Annual/webprogram/Paper232753.html>.
- Drobinski P., and Coauthors, 2014: HyMeX: a 10-year multidisciplinary program on the Mediterranean water cycle. *Bull. Amer. Meteor. Soc.*, **95**, 1063–1082.
- Ducrocq V., and Coauthors, 2014: HyMeX-SOP1: the field campaign dedicated to heavy precipitation and flash-flooding in the northwestern Mediterranean. *Bull. Amer. Meteor. Soc.*, **95**, 1083–1100.
- Dunion, J. P., G. A. Wick, P. G. Black, and J. Walker, 2018: Sensing hazards with operational unmanned technology: 2015-2016 campaign summary, final report. *NOAA Tech Memo. OAR-UAS-001*, 49 pp.
- Elsberry, R. L., and P. A. Harr, 2008: Tropical Cyclone Structure (TCS08) field experiment science basis, observational platforms, and strategy. *Asia-Pac. J. Atmos. Sci.*, **44**, 209–231.
- Evans, C., and R. E. Hart, 2008: Analysis of the wind field evolution associated with the extratropical transition of Bonnie (1998). *Mon. Wea. Rev.*, **136**, 2047–2065.
- Evans, C., and Coauthors, 2017: The extratropical transition of tropical cyclones. Part I: Cyclone evolution and direct impacts. *Mon. Wea. Rev.*, **145**, 4317–4344.
- Foerster, A. M., M. M. Bell, P. A. Harr, and S. C. Jones, 2014: Observations of the eyewall structure of Typhoon Sinlaku (2008) during the transformation stage of extratropical transition. *Mon. Wea. Rev.*, **142**, 3372–3392.
- Frank, W. M., and E. A. Ritchie, 2001: Effects of vertical wind shear on the intensity and structure of numerically simulated hurricanes. *Mon. Wea. Rev.*, **129**, 2249–2269.
- Galarneau, T. J., Jr., L. F. Bosart, and R. S. Schumacher, 2010: Predecessor rain events ahead of tropical cyclones. *Mon. Wea. Rev.*, **138**, 3272–3297.
- Grams, C. M., and H. M. Archambault, 2016: The key role of diabatic outflow in amplifying the midlatitude flow: a representative case study of weather systems surrounding western north Pacific extratropical transition. *Mon. Wea. Rev.*, **144**, 3847–3869.

- Grams, C. M., and S. R. Blumer, 2015: European high-impact weather caused by the downstream response to the extratropical transition of North Atlantic Hurricane Katia (2011). *Geophys. Res. Lett.*, **42**, 8738–8748.
- Grams, C. M., S. C. Jones, C. A. Davis, P. A. Harr, and M. Weissmann, 2013a: The impact of Typhoon Jangmi (2008) on the midlatitude flow. Part I: Upper-level ridgebuilding and modification of the jet. *Quart. J. Roy. Meteor. Soc.*, **139**, 2148–2164.
- Grams, C. M., S. C. Jones, and C. A. Davis, 2013b: The impact of Typhoon Jangmi (2008) on the midlatitude flow. Part II: Downstream evolution. *Quart. J. Roy. Meteor. Soc.*, **139**, 2165–2189.
- Grams, C. M., S. T. K. Lang, and J. H. Keller, 2015: A quantitative assessment of the sensitivity of the downstream midlatitude flow response to extratropical transition of tropical cyclones. *Geophys. Res. Lett.*, **42**, 2015GL065764.
- Grazzini, F., and F. Vitart, 2015. Atmospheric predictability and Rossby wave packets. *Quart. J. Roy. Meteor. Soc.*, **141**, 2793–2802.
- Griffin, K. S., and L. F. Bosart, 2014: The extratropical transition of Tropical Cyclone Edisoana (1990). *Mon. Wea. Rev.*, **142**, 2772–2793.
- Harr, P. A., D. Anwender, and S. C. Jones, 2008: Predictability associated with the downstream impacts of the extratropical transition of tropical cyclones: Methodology and a case study of Typhoon Nabi (2005). *Mon. Wea. Rev.*, **136**, 3205–3225.
- Hart, R. E., 2003: A cyclone phase space derived from thermal wind and thermal asymmetry. *Mon. Wea. Rev.*, **131**, 585–616.
- Hart, R. E., J. L. Evans, and C. Evans, 2006: Synoptic composites of the extratropical transition life cycle of North Atlantic tropical cyclones: Factors determining post-transition evolution. *Mon. Wea. Rev.*, **134**, 553–578.
- Holland, G. J., 1980: An analytic model of the wind and pressure profiles in hurricanes. *Mon. Wea. Rev.*, **108**, 1212–1218.
- Horn, M. and Coauthors, 2014: Tracking scheme dependence of simulate tropical cyclone response to idealized climate simulations. *J. Climate*, **27**, 9197–9213.
- Jones, S. C. and Coauthors, 2003: The extratropical transition of tropical cyclones: forecast challenges, current understanding, and future directions. *Wea. Forecasting*, **18**, 1052–1092.
- Jung, C., and G. M. Lackmann, 2018: Future projections of a recurving TC undergoing ET in a warming climate using a single event case study (Irene 2011). *J. Climate.*, submitted.
- Katsumata, M., S. Mori, B. Geng, and J. Inoue, 2016: Internal structure of ex-Typhoon Phanfone (2014) under an extratropical transition as observed by the research vessel Mirai. *Geophys. Res. Lett.*, **43**, 9333–9341.

- Keighton, S., D. K. Miller, D. Holtz, P. D. Moore, L. B. Perry, L. G. Lee, and D. T. Martin, 2016: Northwest flow snow aspects of Hurricane Sandy. *Wea. Forecasting*, **31**, 173-195.
- Keller, J. H., 2017: Amplification of the downstream wave train during extratropical transition: Sensitivity studies. *Mon. Wea. Rev.*, **145**, 1529–1548.
- Keller, J. H., and C. M. Grams, 2015: The extratropical transition of Typhoon Choi-Wan (2009) and its role in the formation of North American high impact weather. Abstract, *17th Cyclone Workshop*, Pacific Grove, CA, USA.
- Keller, J. H., S. C. Jones, and P. A. Harr, 2014: An eddy kinetic energy view of physical and dynamical processes in distinct forecast scenarios for the extratropical transition of two tropical cyclones. *Mon. Wea. Rev.*, **142**, 2751–2771.
- Keller, J. H., and coauthors, 2019: The extratropical transition of tropical cyclones. Part II: interaction with the midlatitude flow, downstream impacts and implications for predictability. *Mon. Wea. Rev.*, accepted pending minor revisions.
- Kitabatake, N., and F. Fujibe, 2009: Relationship between surface wind fields and three-dimensional structures of tropical cyclones landfalling in the main islands of Japan. *J. Meteor. Soc. Japan*, **87**, 959–977.
- Kitabatake, N., H. Tsuguti and T. Kato, 2017: Effects of synoptic-scale environmental flows on the heavy rainfall event in the Kanto and Tohoku District in September 2015 (in Japanese). *Tenki*, **64**, 887-899.
- Klein, P. M., P. A. Harr, and R. L. Elsberry, 2000: Extratropical transition of western North Pacific tropical cyclones: An overview and conceptual model of the transformation stage. *Wea. Forecasting*, **15**, 373-395.
- Knaff, J.A., C.R. Sampson, and G. Chirokova, 2017: A Global Statistical–Dynamical Tropical Cyclone Wind Radii Forecast Scheme. *Wea. Forecasting*, **32**, 629–644.
- Kossin, J. P., K. A. Emanuel, and G. A. Vecchi, 2014: The poleward migration of the location of tropical cyclone maximum intensity. *Nature*, **509**, doi:10.1038/nature13278.
- Kossin, J. P., K. A. Emanuel, and S. J. Camargo, 2016: Past and projected changes in western North Pacific tropical cyclone exposure. *J. Climate*, **29**, 5725–5739.
- Knapp, K. R., M. C. Kruk, D. H. Levinson, H. J. Diamond, and C. J. Neumann, 2010: The International Best Track Archive for Climate Stewardship (IBTrACS): Unifying tropical cyclone best track data. *Bull. Amer. Meteor. Soc.*, **91**, 363-376.
- Knutson, T. R., J. J. Sirutis, S. T. Garner, G. A. Vecchi, and I. M. Held, 2008: Simulated reduction in Atlantic hurricane frequency under twenty-first-century warming conditions. *Nat. Geosci.*, **1**, 359.
- Knutson, T. R., and Coauthors, 2010: Tropical cyclones and climate change. *Nat. Geosci.*, **3**, 157–163.
- Lackmann, G. M., 2015: Hurricane Sandy before 1900 and after 2100. *Bull. Amer. Meteor. Soc.*, **96**, 547–560.

- Landsea, C. W., G. A. Vecchi, L. Bengtsson, and T. R. Knutson, 2010: Impact of duration thresholds on Atlantic tropical cyclone counts. *J. Climate*, **23**, 2508–2519.
- Leonardo, N. M., and B. A. Colle, 2017: Verification of multimodel ensemble forecasts of North Atlantic tropical cyclones. *Wea. Forecasting*, **32**, 2083–2101.
- Liu, M., and J. A. Smith, 2016: Extreme rainfall from landfalling tropical cyclones in the eastern United States: Hurricane Irene (2011). *J. Hydrometeor.*, **17**, 2883–2904.
- Liu, M., G. A. Vecchi, J. A. Smith, and H. Murakami, 2017: The present-day simulation and twenty-first-century projection of the climatology of extratropical transition in the North Atlantic. *J. Climate*, **30**, 2739–2756.
- Liu, M., G. A. Vecchi, J. A. Smith, and H. Murakami, 2018: Projection of landfalling-tropical cyclone rainfall in the eastern United States under anthropogenic warming. *J. Climate*, **31**, 7269–7286.
- Loridan, T., E. Scherer, M. Dixon, E. Bellone, and S. Khare, 2014: Cyclone wind field asymmetries during extratropical transition in the western North Pacific. *J. Appl. Meteor. Climatol.*, **53**, 421–428.
- Loridan, T., S. Khare, E. Scherer, M. Dixon, and E. Bellone, 2015: Parametric modeling of transitioning cyclone wind fields for risk assessment studies in the western North Pacific. *J. Appl. Meteor. Climatol.*, **54**, 624–642.
- Loridan, T., R.P. Crompton, and E. Dubossarsky, 2017: A machine learning approach to modeling tropical cyclone wind field uncertainty. *Mon. Wea. Rev.*, **145**, 3203–3221.
- Magnusson, L., J. Bidlot, S. T. Lang, A. Thorpe, N. Wedi, and M. Yamaguchi, 2014: Evaluation of medium-range forecasts for Hurricane Sandy. *Mon. Wea. Rev.*, **142**, 1962–1981.
- Manion, A., C. Evans, T. L. Olander, C. S. Velden, and L. D. Grasso, 2015: An evaluation of advanced Dvorak technique-derived tropical cyclone intensity estimates during extratropical transition using synthetic satellite imagery. *Wea. Forecasting*, **30**, 984–1009.
- Marks, F. D., Jr., R. A. Houze Jr., and J. F. Gamache, 1992: Dual-aircraft investigation of the inner core of Hurricane Norbert. Part I: Kinematic structure. *J. Atmos. Sci.*, **49**, 919–942.
- Matyas, C. J., 2013: Processes influencing rain-field growth and decay after tropical cyclone landfall in the United States. *J. Appl. Meteor. Climatol.*, **52**, 1085–1096.
- Matyas, C. J., 2017: Comparing the spatial patterns of rainfall and atmospheric moisture among tropical cyclones having a track similar to hurricane Irene (2011). *Atmosphere*, **8**, 165.
- McTaggart-Cowan, R., L. F. Bosart, J. R. Gyakum, and E. H. Atallah, 2007: Hurricane Katrina (2005). Part I: Complex life cycle of an intense tropical cyclone. *Mon. Wea. Rev.*, **135**, 3905–3926.
- Melhauser, C. and F. Zhang, 2012: Practical and Intrinsic Predictability of Severe and Convective Weather at the Mesoscales. *J. Atmos. Sci.*, **69**, 3350–3371.

- Michaelis, A., and G. Lackmann, 2018: High-resolution global simulations using the Model for Prediction Across Scales (MPAS) for use in studying climate change effects on the extratropical transition of tropical cyclones. *Preprints, 33rd Conference on Hurricanes and Tropical Meteorology*, Ponte Vedra, Florida.
- Milrad, S. M., E. H. Atallah, and J. R. Gyakum, 2009: Dynamical and precipitation structures of poleward-moving tropical cyclones in eastern Canada, 1979-2005. *Mon. Wea. Rev.*, **137**, 836–851.
- Milrad, S. M., E. H. Atallah, and J. R. Gyakum, 2013: Precipitation modulation by the Saint Lawrence River Valley in association with transitioning tropical cyclones. *Wea. Forecasting*, **28**, 331–352.
- Milrad, S. M., E. H. Atallah, J. R. Gyakum, and J. Klepaczki, 2018: The Extreme Precipitation Index (EPI): A diagnostic metric for floods associated with atmospheric flow stagnation. *Wea. Forecasting*, submitted.
- Mokhov, I., E. Dobryshman, and M. Makarova, 2014: Transformation of tropical cyclones into extratropical: The tendencies of 1970–2012. *Doklady Earth Sciences*, **454**, 59–63.
- Munsell, E., J. A. Sippel, S. A. Braun, Y. Weng, and F. Zhang, 2015: Dynamics and predictability of Hurricane Nadine (2012) evaluated through convection-permitting ensemble analysis and forecasts. *Mon. Wea. Rev.*, **143**, 4514–4532.
- Munsell, E. B., and F. Zhang, 2014: Prediction and uncertainty of Hurricane Sandy (2012) explored through a real-time cloud-permitting ensemble analysis and forecast system assimilating airborne Doppler radar observations. *Adv. Model. Earth Syst.*, **6**, 38–58.
- Nuissier O, B. Joly, A. Joly, V. Ducrocq and P. Arbogast, 2011. A statistical downscaling to identify the large-scale circulation patterns associated with heavy precipitation events over southern France. *Quart. J. Roy. Meteor. Soc.*, **137**, 1812–1827.
- Pantillon, F., J.-P. Charboureau, C. Lac, and P. Mascart, 2013: On the role of a Rossby wave train during the extratropical transition of Hurricane Helene (2006). *Quart. J. Roy. Meteor. Soc.*, **139**, 370–386.
- Pantillon, F., J.-P. Chaboureau, and E. Richard, 2015: Remote impact of North Atlantic hurricanes on the Mediterranean during episodes of intense rainfall in autumn 2012. *Quart. J. Roy. Meteor. Soc.*, **141**, 967–978.
- Pantillon, F., J.-P. Chaboureau, and E. Richard, 2016: Vortex–vortex interaction between Hurricane Nadine (2012) and an Atlantic cut-off dropping the predictability over the Mediterranean. *Quart. J. Roy. Meteor. Soc.*, **142**, 419–432.
- Pelly, J. L., and B. J. Hoskins, 2003: A new perspective on blocking. *J. Atmos. Sci.*, **60**, 743–760.
- Pinto, J. M., M. Klawa, U. Ulbrich, S. Ruradi, and P. Speth, 2001: Extreme precipitation events over northwest Italy and their relationship with tropical-extratropical interactions over the Atlantic: Mediterranean Storms., *Baja Sardinia, Italy*, 327–332.

- Pohorsky, R., 2018: A climatological analysis of downstream precipitation extremes associated with recurving North Atlantic tropical cyclones. M.S. Thesis, University of Bern, 87pp, available online at <http://occrdata.unibe.ch/students/theses/msc/219.pdf>.
- Quinting, J. F., and S. C. Jones, 2016: On the impact of tropical cyclones on Rossby wave packets: A climatological perspective. *Mon. Wea. Rev.*, **144**, 2021–2048.
- Quinting, J. F., M. M. Bell, P. A. Harr, and S. C. Jones, 2014: Structural characteristics of T-PARC Typhoon Sinlaku during its extratropical transition. *Mon. Wea. Rev.*, **142**, 1945–1961.
- Reasor, P. D., M. D. Eastin, and J. F. Gamache, 2009: Rapidly intensifying Hurricane Guillermo (1997). Part I: Low-wavenumber structure and evolution. *Mon. Wea. Rev.*, **137**, 603–631.
- Reynolds, C. A., J. D. Doyle, and C. Amerault, 2012: Tropical-extratropical interactions illuminated through adjoint studies. Presentation at the World Weather Ocean Science Conference, Montreal, Canada, 16–21 August 2014.
- Riboldi, J., M. Röthlisberger, and C.M. Grams, 2018: Rossby wave initiation by recurving tropical cyclones in the western north Pacific. *Mon. Wea. Rev.*, **146**, 1283–1301.
- Riemer, M., and S. C. Jones, 2010: The downstream impact of tropical cyclones on a developing baroclinic wave in idealized scenarios of extratropical transition. *Quart. J. Roy. Meteor. Soc.*, **136**, 617–637.
- Riemer, M., and S. C. Jones, 2014: Interaction of a tropical cyclone with a high-amplitude, mid-latitude wave pattern: Waviness analysis, trough deformation and track bifurcation. *Quart. J. Roy. Meteor. Soc.*, **140**, 1362–1376.
- Ritchie, E. A., and R. L. Elsberry, 2001: Simulations of the transformation stage of the extratropical transition of tropical cyclones. *Mon. Wea. Rev.*, **129**, 1462–1480.
- Ritchie, E. A., and R. L. Elsberry, 2007: Simulations of the extratropical transition of tropical cyclones: Phasing between the upper-level trough and tropical cyclone. *Mon. Wea. Rev.*, **135**, 862–876.
- Rogers, R. F., and Coauthors, 2013: NOAA’s Hurricane Intensity Forecasting Experiment: A progress report. *Bull. Amer. Meteor. Soc.*, **94**, 859–882.
- Schäfler, A., and coauthors, 2018: The North Atlantic Waveguide and Downstream Impact Experiment. *Bull. Amer. Meteor. Soc.*, **99**, 1607–1637.
- Schär, C., C. Frei, D. Lüthi, and H. C. Davies, 1996: Surrogate climate-change scenarios for regional climate models. *Geophys. Res. Lett.*, **23**, 669–672.
- Scheck, L., S. C. Jones, and M. Juckes, 2011: The resonant interaction of a tropical cyclone and a tropopause front in a barotropic model. Part II: Frontal waves. *J. Atmos. Sci.*, **68**, 405–419.
- Sharmila, S., and K. J. E. Walsh, 2018: Recent poleward shift of tropical cyclone formation linked to Hadley cell expansion. *Nature Clim. Change*, **8**, 730–736.

- Shaw, T., and Coauthors, 2016: Storm track processes and the opposing influences of climate change. *Nat. Geosci.*, **9**, 656.
- Studholme, J., and S. Gulev, 2018: Concurrent changes to Hadley circulation and the meridional distribution of tropical cyclones. *J. Climate*, **31**, 4367–4389.
- Torn, R. D., 2017: A Comparison of the downstream predictability associated with ET and baroclinic cyclones. *Mon. Wea. Rev.*, **145**, 4651–4672.
- Torn, R. D., and G. J. Hakim, 2015: Comparison of wave packets associated with extratropical transition and winter cyclones. *Mon. Wea. Rev.*, **143**, 1782–1803.
- Torn, R. D., J. S. Whitaker, P. Pegion, T. M. Hamill, and G. J. Hakim, 2015: Diagnosis of the source of GFS medium-range track errors in Hurricane Sandy (2012). *Mon. Wea. Rev.*, **143**, 132–152.
- Towey, K. L., J. F. Booth, A. Frei, and M. R. Sinclair, 2018: Track and circulation analysis of tropical and extratropical cyclones that cause strong precipitation and streamflow events in the New York City watershed. *J. Hydrometeor.*, **19**, 1027–1042.
- Tsuguti, H., T. Kato, and N. Kitabatake, 2016: Factors of the heavy rainfall outbreak in the Kanto and Tohoku District in September 2015 (in Japanese). *Preprints, Spring Meeting of the Meteorological Society of Japan*, B202.
- Uhlhorn, E. W., B. W. Klotz, T. Vukicevic, P. D. Reasor, and R. F. Rogers, 2014: Observed hurricane wind speed asymmetries and relationships to motion and environmental shear. *Mon. Wea. Rev.*, **142**, 1290–1311.
- Waliser, D. E., and coauthors, 2012: The “Year” of Tropical Convection (May 2008–April 2010): Climate variability and weather highlights. *Bull. Amer. Meteor. Soc.*, **93**, 1189–1218.
- Walsh, K. J. E., and Coauthors, 2015: Hurricanes and climate: the U.S. CLIVAR working group on hurricanes. *Bull. Amer. Meteor. Soc.*, **96**, 997–1017.
- Walsh, K. J. E., and Coauthors, 2016: Tropical cyclones and climate change. *WIREs Clim. Change*, **7**, 65–89.
- Wehner, M. F., Prabhat, K. A. Reed, D. Stone, W. D. Collins, and J. T. Bacmeister, 2015: Resolution dependence of future tropical cyclone projections of CAM5.1 in the US CLIVAR hurricane working group idealized configurations. *J. Climate*, **28**, 3905–3925.
- Wehner, M. F., C. M. Zarzycki, and C. Patricola, 2018: Estimating the human influence on tropical cyclone intensity as the climate changes. *Hurricane Risk*, J. M. Collins, and K. Walsh, Eds., Springer International Publishing.
- Weng, Y., and F. Zhang, 2016: Advances in convection-permitting tropical cyclone analysis and prediction through EnKF assimilation of reconnaissance aircraft observations. *J. Meteor. Soc. Japan*, **94**, 345–358.
- Willoughby, H. E., R. W. R. Darling, and M. E. Rahn, 2006: Parametric representation of the primary hurricane vortex. Part II: A family of sectionally continuous profiles. *Mon. Wea. Rev.*, **134**, 1102–1120.

- Wirth, V., M. Riemer, E. K. M. Chang and O. Martius, 2018: Rossby wave packets on the midlatitude waveguide – a review. *Mon. Wea. Rev.*, **146**, 1965-2001.
- Wu, C. C., and coauthors, 2005: Dropsonde Observations for Typhoon Surveillance near the Taiwan Region (DOTSTAR): An overview. *Bull. Amer. Meteor. Soc.*, **86**, 787–790.
- Yoshida, K., M. Sugi, R. Mizuta, H. Murakami, and M. Ishii, 2017: Future changes in tropical cyclone activity in high-resolution large-ensemble simulations. *Geophys. Res. Lett.*, **44**, 9910-9917.
- Zarzycki, C. M., D. R. Thatcher, and C. Jablonowski, 2017: Objective tropical cyclone extratropical transition detection in high-resolution reanalysis and climate model data. *Adv. Model. Earth Syst.*, **9**, 130–148.
- Zarzycki, C. M., and P. A. Ullrich, 2017: Assessing sensitivities in algorithmic detection of tropical cyclones in climate data. *Geophys. Res. Lett.*, **44**, 1141–1149.
- Zhang, F., and Y. Weng, 2015: Predicting hurricane intensity and associated hazards: A five-year real-time forecast experiment with assimilation of airborne Doppler radar observations. *Bull. Amer. Meteor. Soc.*, **96**, 25–32.